UNIVERSITY OF ABERDEEN

THE DEVELOPMENT OF A GENERAL METHOD TO MAP BETWEEN CONTINUOUS AND DISCRETE MOLECULAR POTENTIALS

CHRISTOPHER JAMES THOMSON

2012

THIS THESIS WAS SUBMITTED AS PART OF THE REQUIREMENT FOR THE MENG. DEGREE IN ENGINEERING.

School of Engineering 2012 Univ. of Aberdeen

ABSTRACT

Molecular interactions are frequently described using either continuous or discrete intermolecular potentials. The objective of this dissertation is to develop a general technique for converting continuous molecular models to discrete forms. Discrete models have many desirable properties; they allow the use of event-driven molecular dynamics, which is more accurate and stable than traditional techniques. Discrete potentials also have a set of well-developed theories allowing accurate predictions of the equations of state and transport properties.

An event-driven and a force-driven simulator are developed for this dissertation to test the effectiveness of number of proposed conversion methods. A novel technique is proposed, which appears to accurately reproduce the thermodynamics of the original continuous potentials. This technique opens the door to rapid and accurate predictions of thermophysical properties from existing molecular interactions found in the literature.

CONTENTS

Final word count: 10741

LIST OF FIGURES

LIST OF TABLES

NOMENCLATURE

Acronyms/Terminology

CHARMM Chemistry at HARvard Molecular Mechanics, 6

FCC Face Centred Cubic, 19

MD Molecular Dynamics, 1

RDF Radial Distribution Function, 28

SPEADMD Step Potentials for Equilbria And Discontinuous Molecular Dynamics, 9

TPT Thermodynamic Perturbation Theory, 2

Functions

$f(v_x)$ Probability distribution of equilibrium velocities, 27

F_E Magnitude of the Expected Force, 35

$g(r)$ Radial distribution function, 28

$y(r)$ Indirect Correlation Function, 29

Z Partition function, 35

Operators

∇ Gradient operator, 5

Notation

$\bar{x}$ Mean value, 27

$\hat{x}$ Unit vector, 17

$\langle\ \rangle$ Time average, 25

x^* Reduced quantity, 32

Variables/Constants

β Reciprocal of the reduced temperature, 35

$\Delta\mathbf{v}_i$ Change in the velocity of particle i during a collision, 17

$\Delta\Phi$ Change in potential energy during a collision, 17

Δt Simulator time increment, 13

$\mathbf{a}_i$ Acceleration vector of particle i, 5

$\mathbf{r}_i$ Position vector of particle i, 12

$\mathbf{r}_{ij}$ Separation vector between particles i and j, 16
$\mathbf{v}_i$ Velocity vector of particle i, 13
$\mathbf{v}_{ij}$ Relative velocity between particles i and j, 16
Φ Potential Energy of the system, 27
Φ_{ij} Intermolecular potential between particles i and j, 5
ρ Density of the system, 28
σ Characteristic length, taken to be particle diameter, 6
τ Dummy time variable in time average integrals, 25
ε Characteristic energy, usually well depth, 6
A Momentum change during a collision, 18
B_n n^{th} Virial coefficient, 28
c_n n^{th} Gear coefficient, 14
E_K Kinetic energy of the system, 27
F_i Force acting on particle i, 5
F_{ij} Intermolecular force between particle i and j, 5
k_B Boltzmann Constant, 27
M Number of measurements taken, 26
m_i Mass of a particle i, 5
N Number of particles in the system, 5
P Pressure of the system, 28
r Distance between two particles, 6
T Temperature of the system, 20
t Time, 12
t_c Time between collisions, 25
U Total internal energy of the system, 27
V Volume of the system, 20

ACKNOWLEDGEMENTS

Firstly, I would like to thank my supervisor Dr. Marcus Bannerman for introducing me to the world of molecular dynamics. Without his seemingly infinite amounts of patience, enthusiasm and wisdom, this dissertation would not have been possible.

I would like to thank my family for their continual support, and for donating their computers which allowed me to run the many simulations required to complete this project. I would also like to thank my father for taking the time to help proof-read this dissertation.

CHAPTER

ONE

INTRODUCTION

Process simulation packages have become an integral part of chemical engineering design. Central to these simulation software packages is the ability to calculate thermodynamic and transport properties of fluids quickly and accurately. Many modern processes require knowledge of molecular behaviour, such as diffusion through nano-porous materials, or membranes important to separation and catalysis [1], or chemical reaction rates.

In order to predict the macroscopic behaviour of fluids, an understanding of the interactions at the molecular level is important. The problem is that experimentation at this small a scale is difficult. Experimental techniques such as X-ray crystallography rely on a theoretical understanding of the system; however, theoretical analysis of this level is extremely complex and frequently cannot be solved analytically.

Over the past few decades, computer simulation has offered a solution to these problems. Using computers, the motion of a small number of molecules can be predicted; this technique is known as molecular dynamics (MD). The first MD simulations were carried out in the 50's by Alder and Wainwright [2] and popularised by Verlet in 1967 [3]. These early simulations were limited to tens or hundreds of particles, whereas modern day supercomputers are now capable of simulating systems of billions of particles for long periods of time [4]. These simulations allow not only the prediction of thermodynamic and transport properties but help develop the basic understanding of these micro-scale systems. Computational simulations can also access conditions such as very high/low temperatures or pressures, which are impractical to investigate experimentally [5].

These simulations rely on intermolecular potentials to model interactions between atoms or molecules. These potentials fall into two mathematical categories: continuous and discrete. Discrete potentials have two useful properties, firstly, they allow Newton's Equation of Motion to be integrated analytically and therefore the results are accurate to machine precision. The other useful aspect of discrete potentials is that an equation of state to describe behaviour of fluids can be created theoretically using Thermodynamic

Perturbation Theory (TPT) [6, 7]. This is currently a major focus point of discrete potential research [8–11] and equations of state have been created for hydrocarbons that compare well with experimental values [10, 11]. However, most of the research done on intermolecular potentials has been on the development of continuous potentials such as CHARMM [12], AMBER [13] and COMPASS [14]. If a general method to convert continuous potentials to equivalent discrete potentials could be developed, the extensive literature on continuous potentials could be combined with the advantages of discrete potentials.

There have already been several attempts to create discrete potentials equivalent to popular continuous potentials, most of these have been created by hand [10, 11, 15] . While these potentials compare very well to the corresponding continuous potentials, they are very time consuming to create and do not adapt to changes in temperature. Some simple automatic methods to create discontinuous potentials have been suggested but these usually involve a simple stepping scheme such as placing the discontinuities evenly. However, this method only works well if large numbers of discontinuities are used [9] but more discontinuities means a longer run time for the simulation, which is undesirable. The aim of this dissertation is to create a novel potential conversion method that automatically fixes discontinuity parameters yet works accurately even with low numbers of steps.

This dissertation will first cover the discrete and continuous potentials used to model molecular interactions (Chap. 2). Then the techniques used in MD simulations are described in Chap. 3. In order to compare potentials, measurements of properties need to be made during the simulations, the methods used to achieve this is discussed in Chap. 4. Chapter 5 will cover the techniques that will be investigated to find the best potential conversion method. The results of which will be discussed in Chap. 6. Finally, the results of the dissertation is summarised and suggestions for further work are presented in Chap. 7.

1.1 References

[1] Maginn, E. J.; Elliott, J. R. Historical Perspective and Current Outlook for Molecular Dynamics As a Chemical Engineering Tool. *Ind. Eng. Chem. Res.* **2010**, *49*, 3059–3078, DOI: 10.1021/ie901898k.

[2] Alder, B. J.; Wainwright, T. E. Phase Transition for a Hard Sphere System. *J. Chem. Phys.* **1957**, *27*, 1208–1209, DOI: 10.1063/1.1743957.

[3] Verlet, L. Computer "Experiments" on Classical Fluids. I. Thermodynamical Properties of Lennard-Jones Molecules. *Phys. Rev.* **1967**, *159*, 98–103, DOI: 10.1103/PhysRev.159.98.

[4] Allsopp, N.; Ruocco, G.; Fratalocchi, A. Molecular Dynamics Beyonds the Limits: Massive Scaling on 72 Racks of a BlueGene/P and Supercooled Glass Dynamics of a 1 Billion Particles System. *J. Comput. Phys.* **2012**, *231*, 3432–3445, DOI: 10.1016/j.jcp.2012.01.019.

[5] Mandumpal, J. B.; Kreck, C. A.; Mancera, R. L. A Molecular Mechanism of Solvent Cryoprotection in Aqueous DMSO Solutions. *Phys. Chem. Chem. Phys.* **2011**, *13*, 3839–3842, DOI: 10.1039/C0CP02326D.

[6] Benavides, A. L.; Gil-Villegas, A. The Thermodynamics of Molecules with Discrete Potentials. *Mol. Phys.* **1999**, *97*, 1225–1232, DOI: 10.1080/00268979909482924.

[7] Barker, J. A.; Henderson, D. Perturbation Theory and Equation of State for Fluids: The Square-Well Potential. *J. Chem. Phys.* **1967**, *47*, 2856–2861, DOI: 10.1063/1.1712308.

[8] Vidales, A.; Benavides, A. L.; Gil-Villegas, A. Perturbation Theory for Mixtures of Discrete Potential Fluids. *Mol. Phys.* **2001**, *99*, 703–710, DOI: 10.1080/00268970010018846.

[9] Chapela, G.; Rio, F. del; Benavides, A. L.; Alejandre, J. Discrete Perturbation Theory Applied to Lennard-Jones and Yukawa Potentials. *J. Chem. Phys.* **2010**, *133*, 234107.

[10] Elliot Jr., J. R. Optimized Step Potential Models for n-Alkanes and Benzene. *Fluid Phase Equilib.* **2002**, *194-197*, 161–168, DOI: 10.1016/S0378-3812(01)00664-1.

[11] Unlu, O.; Gray, N. H.; Gerek, Z. N.; Elliott, J. R. Transferable Step Potentials for the Straight-Chain Alkanes, Alkenes, Alkynes, Ethers, and Alcohols. *Ind. Eng. Chem. Res.* **2004**, *43*, 1788–1793, DOI: 10.1021/ie034036m.

[12] MacKerell, A. D. et al. All-Atom Empirical Potential for Molecular Modeling and Dynamics Studies of Proteins. *J. Phys. Chem. B* **1998**, *102*, 3586–3616, DOI: 10.1021/jp973084f.

[13] Ponder, J. W.; Case, D. A. In *Protein Simulations*, Daggett, V., Ed.; Advances in Protein Chemistry, Vol. 66; Academic Press: 2003, pp 27 –85, DOI: 10.1016/S0065-3233(03)66002-X.

[14] McQuaid, M. J.; Sun, H.; Rigby, D. Development and Validation of COMPASS Force Field Parameters for Molecules with Aliphatic Azide Chains. *J. Comput. Chem.* **2004**, *25*, 61–71, DOI: 10.1002/jcc.10316.

[15] Chapela, G.; Scriven, L. E.; Davis, H. T. Molecular Dynamics for Discontinuous Potential. IV. Lennard-Jonesium. *J. Chem. Phys.* **1989**, *91*, 4307, DOI: 10.1063/1.456811.

CHAPTER

TWO

MOLECULAR MODELS

In this chapter, the dynamics and models used to represent molecular systems are discussed. First, the arguments for selecting classical mechanics over quantum mechanics as the underlying dynamics for the simulations are presented. Then, the two major classifications of the available classical models, discrete and continuous potentials, are discussed.

2.1 Classical Mechanics

2.1.1 Validity of Classical Mechanics

The underlying assumption behind many molecular dynamics simulations is that the particles move according to the laws of classical mechanics. Strictly, atoms and molecules should be treated using quantum mechanics due to their size and speed. However molecular dynamics makes two assumptions so that these quantum mechanical effects may be ignored.

The first is the Born-Oppenheimer approximation which allows the motion of electrons and the nucleus to be treated separately. Since the nucleus is much larger than the electrons, and hence less affected by quantum mechanics, it is treated as a classical particle.

The second assumption is that any quantum mechanical effects should average out. Molecular dynamics is rarely interested in the motion of a single electron, it is more concerned with the statistical average over every electron. The average effect of electron interactions is approximated by an energetic potential [1].

These assumptions are usually valid unless very light atoms (such as hydrogen or helium) are being simulated, or the particles are vibrating at very high rates [2].

2.1.2 Newton's Second Law of Motion

The fundamental identity of classical mechnanics is Newton's Second Law of Motion (Eq. (2.1.1)):

$$\mathbf{F}_i = m_i \mathbf{a}_i \tag{2.1.1}$$

where $\mathbf{F}_i$ is the force vector acting on particle i, m_i is the mass of the particle and $\mathbf{a}_i$ is the particle's acceleration vector.

This equation allows the prediction of a particle's trajectory provided that an initial position and velocity is known; and the forces acting on that particle can be calculated for any position or velocity. If a force depends only on the position of a particle, it is known as a conservative force. Almost all forces considered in molecular dynamics are of this type because atoms or molecules do not lose energy due to friction or any other dissipative process.

Conservative molecular forces can be of one of two types. The first are body forces, which only depend on a single particle's absolute position, such as gravity. However, gravity is usually disregarded in MD as atoms and molecules have such low masses that gravity has very little effect on them over the timescales studied.

The second and most important type are intermolecular forces that depend on position relative to other particles. In general, the intermolecular forces are a function of all particle positions; however, usually the total force acting on a particle i is assumed to be a sum of the forces between i and every other particle j. This is known as the binary interaction assumption and the summation of forces is given by:

$$\mathbf{F}_i = \sum_{j \neq i}^{N} \mathbf{F}_{ij} \tag{2.1.2}$$

where $\mathbf{F}_{ij}$ is the force between particles i and j and N is the total number of particles in the system. Force calculations are limited to pairs as this is simpler, but there are examples of n-body forces in the literature (e.g. see Ref. [3]).

The intermolecular forces used in molecular dynamics are frequently described using a potential. Provided that the force is conservative, it can be calculated from its potential using the following equation:

$$\mathbf{F}_{ij} = -\nabla \Phi_{ij} \tag{2.1.3}$$

where ∇ denotes the gradient of the potential, between particles i and j, Φ_{ij}.

Using this definition, it can be see that by defining an intermolecular potential, the intermolecular forces are also described. In the literature, intermolecular force fields are usually described using potentials and in the following sections the two types of potentials will be discussed.

2.2 Continuous Potentials

Models for the intermolecular interactions are typically defined using functions for the potential energies between molecules. A very popular potential used in molecular dynamics simulations is the Lennard-Jones potential [4] given by the following expression:

$$\Phi(r) = 4\varepsilon \left[\left(\frac{\sigma}{r}\right)^{12} - \left(\frac{\sigma}{r}\right)^{6} \right] \tag{2.2.1}$$

where r is the distance between the particles, ε is the depth of the energy well and σ is the distance where the potential between two particles is zero. A plot of this potential is given in Fig. 2.1. Despite its simplicity, it gives comparable results to experimental values [5] for noble gases due to their monatomic nature.

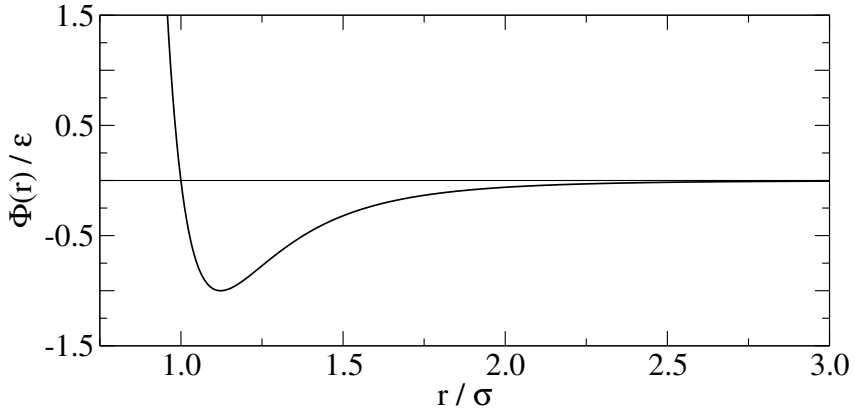

Figure 2.1: Plot of the Lennard-Jones potential.

The power 12 term, $(\sigma/r)^{12}$, gives the potential a repulsive core caused by Pauli repulsion of overlapping electron shells. This repulsion is more accurately represented by an exponential function which forms the basis of the Buckingham potential [6]. However the Buckingham potential is not as popular as the Lennard-Jones potential because the exponential function is more computationally expensive to calculate [7].

The power 6 term, $(\sigma/r)^{6}$, in the Lennard-Jones potential represents the attractive Van der Waals forces. This attractive well and repulsive core can be seen in the force plot of the Lennard-Jones potential, Fig. 2.2.

While the Lennard-Jones potential simulates interactions between single atoms very well, more complex potentials are needed to describe particle chains. An example of this

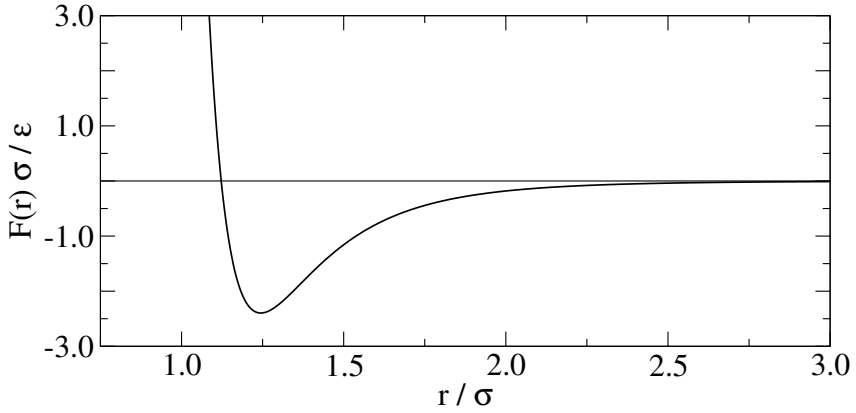

Figure 2.2: Plot of the force between a pair of Lennard-Jones particles separated by a distance r, negative values represent an attractive force, while positive values indicate a repulsive force.

is the CHARMM (Chemistry at HARvard Molecular Mechanics) potential (Eq. (2.2.2)) [8].

$$\begin{aligned}\Phi = &\sum_{\text{bonds}} k_b(r-r_0)^2 + \sum_{UB} K_{UB}(S-S_0)^2 + \sum_{\text{angles}} k_\theta(\theta-\theta_0)^2 \\ &+ \sum_{\text{dihedrals}} k_\chi[1+\cos(n\chi-\delta)] + \sum_{\text{improper}} k_\psi(\psi-\psi_0)^2 \\ &+ \sum_{i=1}^{N-1}\sum_{j>i}^{N}\left\{4\varepsilon\left[\left(\frac{\sigma}{r_{ij}}\right)^{12} - \left(\frac{\sigma}{r_{ij}}\right)^{6}\right] + \frac{q_i q_j}{r_{ij}}\right\}\end{aligned} \tag{2.2.2}$$

Even in this more sophisticated potential, the Lennard-Jones potential is being used to represent Van der Waals forces while Coulomb's Law $\left(\frac{q_i q_j}{r_{ij}}\right)$ is modelling longer range electrostatic interactions. The first five terms of Eq. (2.2.2) are constraints on bond movements (stretching, Urey-Bradley bond vibration, angle bending, dihedral angle, and improper dihedral angle motion respectively, see Ref. [9] for descriptions of these bond movements).

2.3 Discrete Potentials

Discrete potentials differ from continuous potentials because they have discontinuities. The simplest discrete potential is that of the hard sphere (see Fig. 2.3). Hard spheres were the first molecular models ever simulated [10] due to their relative simplicity and are so-named as they cannot penetrate each other due to the infinite overlap energy. The potential for hard spheres is shown in Eq. (2.3.1), where σ is the diameter of the spheres.

$$\Phi(r) = \begin{cases}\infty & \text{if } r < \sigma \\ 0 & \text{if } r \geq \sigma\end{cases} \tag{2.3.1}$$

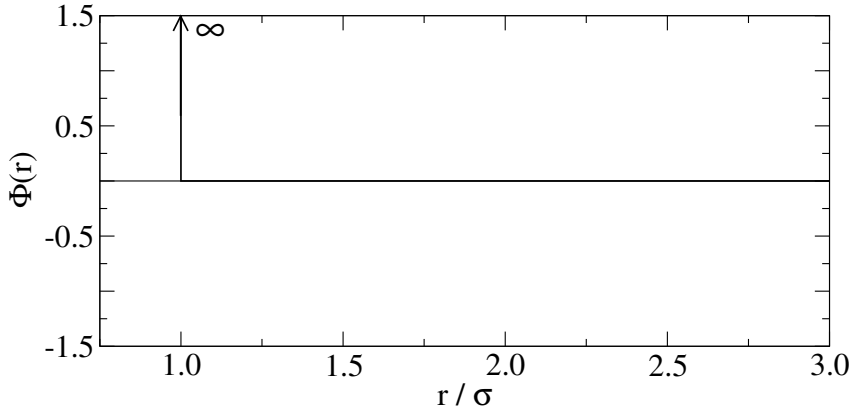

Figure 2.3: Plot of the hard sphere potential.

By calculating the force between two hard spheres using Eq. (2.1.3) shows that hard spheres exert no force until the particles collide whereupon they experience an infinite repulsive force. This means that hard spheres cannot overlap as they would have to exceed an infinite force to do so.

The hard sphere potential can be elaborated upon by adding an attractive well outside the hard core (see Fig. 2.4). This square well potential takes the form of Eq. (2.3.2) [11], where λ is the outer radius of the core in terms of the hard core diameter σ. It should be noted here that at $r = \lambda\sigma$ the particle can have a potential energy of either zero or $-\varepsilon$.

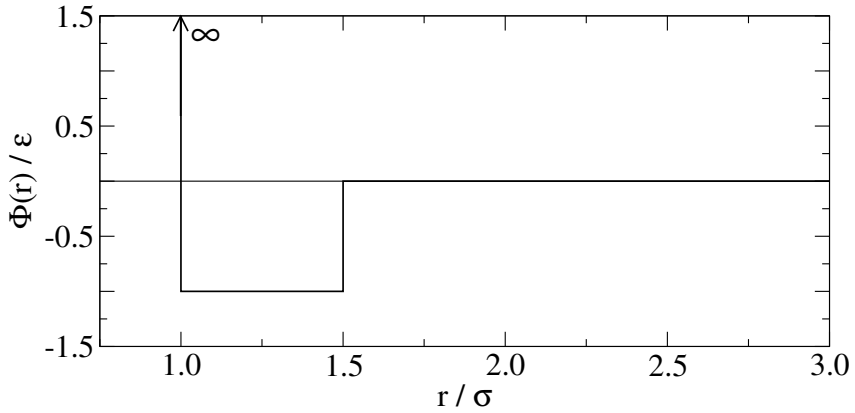

Figure 2.4: Plot of the square well potential with $\lambda = 1.5$

$$\Phi(r) = \begin{cases} \infty & \text{if } r < \sigma \\ -\varepsilon & \text{if } \sigma \leq r \leq \lambda\sigma \\ 0 & \text{if } r \geq \sigma \end{cases} \tag{2.3.2}$$

Stepped potentials are a combination of square wells and square shoulders to mimic the behaviour of a continuous potential. Many types of stepped potentials have been developed in the literature. Chapela *et al.* [12] created a stepped version of the Lennard-

Jones potential shown in Fig. 2.5.

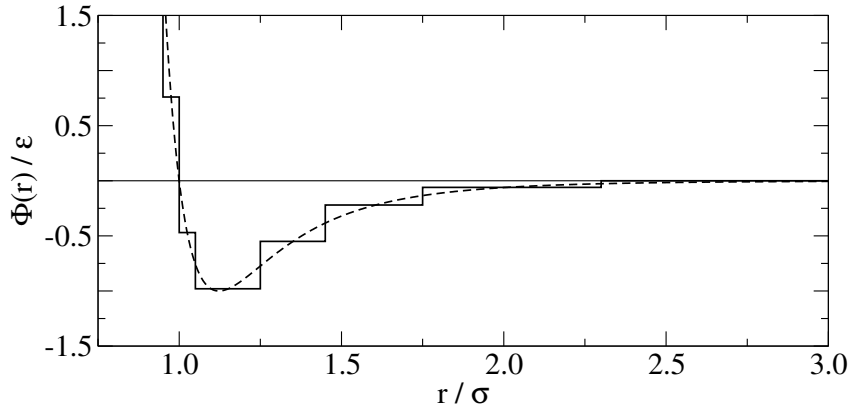

Figure 2.5: A stepped version (solid line) of the continuous Lennard-Jones potential (dashed line) created by Chapela *et al.*

The SPEADMD (Step Potentials for Equilibria And Discontinuous Molecular Dynamics) project has created stepped potentials (see Fig. 2.6) that represent a range of hydrocarbons [13–15]. These potentials have been converted to equations of state using TPT that match experimental values relatively well.

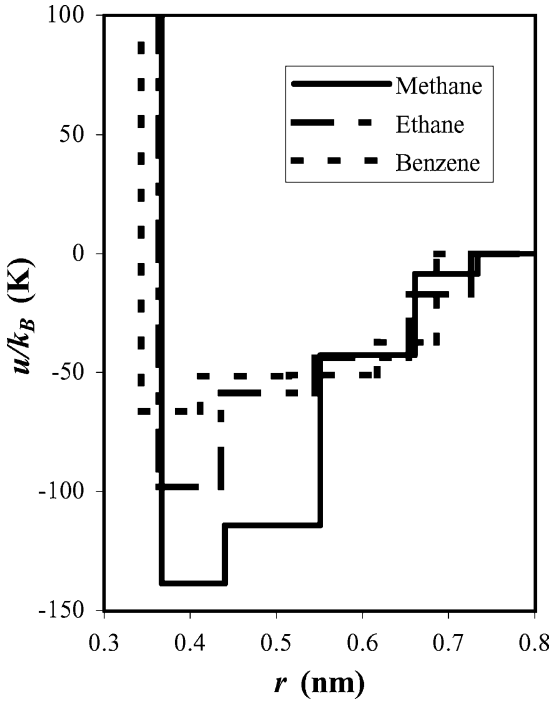

Figure 2.6: SPEADMD stepped potentials for methane, ethane and benzene [13].

There are many validated continuous models in the literature, and these potentials are very advanced. Discrete potentials, on the other hand, are still underdeveloped and underused. In the next chapter the methods used to simulate these potential models will be described.

2.4 References

[1] Jasper, A. W.; Nangia, S.; Zhu, C.; Truhlar, D. G. Non-Born - Oppenheimer Molecular Dynamics. *Acc. Chem. Res.* **2006**, *39*, 101–108, DOI: 10.1021/ar040206v.

[2] Frenkel, D.; Smit, B., *Understanding Molecular Simulations*, 2nd Edition; Academic Press: 2002, DOI: 10.1016/B978-012267351-1/50006-7.

[3] Tersoff, J. New Empirical Approach for the Structure and Energy of Covalent Systems. *Phys. Rev. B* **1988**, *37*, 6991–6999, DOI: 10.1103/PhysRevB.37.6991.

[4] Lennard-Jones, J. The Determination of Molecular Fields I & II. *Proc. R. Soc. Lon. Ser-A* **1924**, *106A*, 441–477, DOI: 10.1098/rspa.1924.0081.

[5] Rahman, A Correlations in the Motion of Atoms in Liquid Argon. *Phys. Rev.* **1964**, *136*, A405–A411, DOI: 10.1103/PhysRev.136.A405.

[6] Buckingham, R. A. The Classical Equation of State of Gaseous Helium, Neon and Argon. *Proc. R. Soc. Lon. Ser-A* **1938**, *168*, 264–283, DOI: 10.1098/rspa.1938.0173.

[7] White, D. N. J. A Computationally Efficient Alternative to the Buckingham Potential for Molecular Mechanics Calculations. *J. Comput.-Aided Mol. Des.* **1997**, *11*, 517–521, DOI: 10.1023/A:1007911511862.

[8] MacKerell, A. D. et al. All-Atom Empirical Potential for Molecular Modeling and Dynamics Studies of Proteins. *J. Phys. Chem. B* **1998**, *102*, 3586–3616, DOI: 10.1021/jp973084f.

[9] Spoel, D. van der; Lindahl, E.; Hess, B.; Buuren, A. R van; Apol, E.; Meulenhoff, P.; Tieleman, D. P.; Sijbers, A. L. T. M.; Feenstra, K. A.; Drunen, R. van; Berendsen, H. J. C. Gromacs User Manual version 4.5.4., www.gromacs.org.

[10] Alder, B. J.; Wainwright, T. E. Phase Transition for a Hard Sphere System. *J. Chem. Phys.* **1957**, *27*, 1208–1209, DOI: 10.1063/1.1743957.

[11] Barker, J. A.; Henderson, D. Perturbation Theory and Equation of State for Fluids: The Square-Well Potential. *J. Chem. Phys.* **1967**, *47*, 2856–2861, DOI: 10.1063/1.1712308.

[12] Chapela, G.; Scriven, L. E.; Davis, H. T. Molecular Dynamics for Discontinuous Potential. IV. Lennard-Jonesium. *J. Chem. Phys.* **1989**, *91*, 4307, DOI: 10.1063/1.456811.

[13] Elliot Jr., J. R. Optimized Step Potential Models for n-Alkanes and Benzene. *Fluid Phase Equilib.* **2002**, *194-197*, 161–168, DOI: 10.1016/S0378-3812(01)00664-1.

[14] Unlu, O.; Gray, N. H.; Gerek, Z. N.; Elliott, J. R. Transferable Step Potentials for the Straight-Chain Alkanes, Alkenes, Alkynes, Ethers, and Alcohols. *Ind. Eng. Chem. Res.* **2004**, *43*, 1788–1793, DOI: 10.1021/ie034036m.

[15] Vahid, A.; Elliott Jr., J. R. Transferable Intermolecular Potentials for Carboxylic Acids and their Phase Behavior. *AIChE Journal* **2010**, *56*, 485–505, DOI: 10.1002/aic.11966.

CHAPTER

THREE

MOLECULAR DYNAMICS

In this chapter the principles of molecular dynamics simulations are discussed. First, the techniques used to solve Newton's Second Law of Motion for both continuous and discrete potentials are described. This is followed by a discussion of other important aspects of the molecular simulation programs used in this dissertation.

3.1 Applying Classical Mechanics to Molecular Systems

The most fundamental part of molecular dynamics is solving Newton's Second Law of Motion (Eq. (3.1.1)) for every particle in the system.

$$\mathbf{F}_i = m_i \mathbf{a}_i = m_i \frac{\partial^2 \mathbf{r}_i}{\partial t^2} \tag{3.1.1}$$

In Eq. (3.1.1), $\mathbf{r}_i$ is the position vector of particle i, and t is time. While the forces acting on the particles can be calculated from their intermolecular potentials, the future positions of the particles become the solution of a set of simultaneous differential equations (there are $3N$ differential equations to solve). The techniques used to solve these differential equations are different depending on whether the potential is continuous or discontinuous.

3.2 Force-Driven Simulation

3.2.1 Introduction

For continuous potentials, it is not possible to solve Eq. (3.1.1) analytically for the future position of more than two particles [1]. Therefore numerical methods for solving differential equations have to be used; these are known as numerical integrators.

3.2.2 Integrators

Numerical integrators can be explained using a Taylor series:

$$\mathbf{r}(t+\Delta t) = \mathbf{r}(t) + \frac{\partial \mathbf{r}(t)}{\partial t}(\Delta t) + \frac{1}{2}\frac{\partial^2 \mathbf{r}(t)}{\partial t^2}\Delta t^2 + \frac{1}{3!}\frac{\partial^3 \mathbf{r}(t)}{\partial t^3}\Delta t^3 + \frac{1}{4!}\frac{\partial^4 \mathbf{r}(t)}{\partial t^4}\Delta t^4 + \mathcal{O}(\Delta t^5) \tag{3.2.1}$$

where Δt is the time-step and $\mathcal{O}(\Delta t^5)$ represents the higher order terms.

Although the Taylor series is exact, it is an infinite series which makes it impractical to use. It must be truncated at some order. The simplest integrator is Euler's Method:

$$\mathbf{r}(t+\Delta t) = \mathbf{r}(t) + \Delta t \mathbf{v}(t) + \mathcal{O}(\Delta t^2) \tag{3.2.2a}$$

$$\mathbf{v}(t+\Delta t) = \mathbf{v}(t) + \Delta t \mathbf{a}(t) + \mathcal{O}(\Delta t^2) \tag{3.2.2b}$$

where $\mathbf{v}$ is the velocity vector of the particle and $\mathcal{O}()$ indicates the truncation error in the integrator. However, this method suffers from large errors and is highly unstable (i.e. it amplifies any errors) [2] and is therefore rarely used. The Verlet Integrator [3] improves upon Euler's method by combining the forward time-step with a reverse time-step (Eq. (3.2.3a)). Thihs method is actually third order as the third (and first) derivative are cancelled out during its derivation. The Verlet integrator does not include an equation to calculate the future velocity, as the forces are only a function of position; however, it is often desired to know the velocities to calculate physical properties so the central difference approximation is often used (Eq. (3.2.3b)).

$$\mathbf{r}(t+\Delta t) = 2\mathbf{r}(t) - \mathbf{r}(t-\Delta t) + \mathbf{a}(t)\Delta t^2 + \mathcal{O}(\Delta t^4) \tag{3.2.3a}$$

$$\mathbf{v}(t+\Delta t) = \frac{\mathbf{r}(t+\Delta t) - \mathbf{r}(t-\Delta t)}{2\Delta t} \tag{3.2.3b}$$

Integrators suffer from two key failings that cause a systematic gain of energy known as "energy drift". Firstly, integrators are based on infinite Taylor series which cannot be fully implemented and have to be truncated after a certain number of terms; this introduces truncation error. Secondly, integrators are unable to predict values of forces that have discontinuities in them, such as discrete potentials or discontinuities introduced by truncating potentials to improve simulator speed. There are a couple of types of integrators that try and reduce these problems.

The first method to improve the traditional integrator is the predictor-corrector integrator. These use a truncated Taylor series to calculate a predicted value for the future position and higher order time derivatives. The force is calculated at this predicted position, then the difference between the predicted acceleration, and the corrected acceleration calculated from the force, is used to correct the position and time derivatives.

The most common predictor-corrector integrator is that of Gear [4] using the 5th or-

der algorithm. The predicted value for the n^{th} time derivative is shown in Eq. (3.2.4). By defining $\Delta\mathbf{a} = \mathbf{a}^C - \mathbf{a}^P$, where the superscripts C and P denote the corrected and predicted values respectively, the corrected time derivatives can be calculated using Eq. (3.2.5) with coefficients from Eq. (3.2.6).

$$\frac{\partial^n}{\partial t^n}\mathbf{r}^P(t+\Delta t) = \sum_{k=i}^{5}\frac{1}{k!}\frac{\partial^n}{\partial t^n}\mathbf{r}(t)\Delta t^k + \mathcal{O}(\Delta t^6) \tag{3.2.4}$$

$$\frac{\partial^n}{\partial t^n}\mathbf{r}^C(t+\Delta t) = \frac{\partial^n}{\partial t^n}\mathbf{r}^P(t+\Delta t) + \frac{c_i}{\Delta t^i}\left(\frac{\Delta t^2}{2}\Delta\mathbf{a}\right) \tag{3.2.5}$$

$$XOc_0 = \frac{3}{16},\ \ c_1 = \frac{251}{360},\ \ c_2 = 1,\ \ c_3 = \frac{11}{18},\ \ c_4 = \frac{1}{6},\ \ c_5 = \frac{1}{60} \tag{3.2.6}$$

Gear's algorithm, while more accurate at short time-steps than Verlet's integrator [2], loses precision at long time-steps and is computationally expensive.

The loss of precision at long time-steps is due to energy drift, a failing all the integrators mentioned so far suffer from. This is reduced in another type of integrator: the symplectic integrator. These have the useful property in that they, on average, conserve energy [5]. The most common symplectic integrator used in MD is the Velocity Verlet Integrator [6] shown in Eq. (3.2.7).

$$\mathbf{r}(t+\Delta t) = \mathbf{r}(t) + \mathbf{v}(t)\Delta t + \frac{1}{2}\mathbf{a}(t)\Delta t^2 + \mathcal{O}(\Delta t^4) \tag{3.2.7a}$$

$$\mathbf{v}(t+\Delta t) = \mathbf{v}(t) + \frac{\mathbf{a}(t)+\mathbf{a}(t+\Delta t)}{2}\Delta t \tag{3.2.7b}$$

The popularity of the Velocity Verlet is due to its computational simplicity, accuracy and stability at relatively long time-steps. It can even be expanded [7] to maintain its accuracy and stability at very long time-steps at a small extra computational cost. However the Velocity Verlet cannot be used in systems that do not conserve energy, i.e. systems with dissipative forces.

The Velocity Verlet integrator was chosen as the integrator implemented in the force-driven simulation used in this dissertation. The complexity and high computational cost of Gear's algorithm does not compensate for any slight increase in accuracy over the Velocity Verlet integrator. Also since all the forces considered in this dissertation are conservative, the use of a symplectic integrator over non-symplectic integrators such as Gear's algorithm or the Verlet integrator is sensible.

3.2.3 General Algorithm

The general algorithm for a force-driven simulator has not changed since they were first introduced by Rahman [8] who predicted physical properties of liquid argon using a Lennard-Jones potential.

Force-driven simulators move through time in uniform intervals of time, Δt. The particles' positions are calculated at the end of each interval. These new positions can then be used to calculate the new forces acting on the particles. The overall algorithm for the force-driven simulator written for this dissertation can be summarised as follows:

1. Initialisation.
2. Calculate particles' future positions using a numerical integrator (Velocity Verlet).
3. Calculate the forces acting on the particles from the intermolecular potential (Lennard-Jones).
4. Calculate the future velocities of particles .
5. Run thermostat.
6. Measure properties .
7. Repeat steps 2-6 for the desired number of iterations.

The techniques used to measure the physical properties of the system will be discussed in Chap. 4. The other parts of the algorithm such as initialising the system and the thermostat will be discussed in more depth later in this chapter, but first, the solution of Newton's Equation of Motion for discontinuous potentials is described.

3.3 Event-driven Simulation

3.3.1 Introduction

The methods for integrating continuous potentials rely on calculating the forces acting on the particles, however this is problematic when working with discrete potentials. The gradient (and hence the force) is either infinite at the steps, or zero in between them.

Therefore a new technique for simulating these discrete potentials is needed. There is no force between the steps therefore the acceleration is zero (Eq. (3.3.1)).

$$\mathbf{F}_i = m_i \mathbf{a}_i = 0 \tag{3.3.1}$$

This can be integrated analytically to give:

$$\mathbf{r}_i(t + \Delta t) = \mathbf{r}_i + \mathbf{v}_i \Delta t \tag{3.3.2}$$

which allows the prediction of when particles reach a step, and using the conservation of energy and momentum, the post collision velocities of the particles can be calculated (this is expanded upon in Sec. 3.3.3). This method is known as event-driven molecular

dynamics and is an analytical solution of Newton's Second Law of Motion. This means that event-driven simulators do not suffer from the numerical errors associated with the numerical integrators described in Sec. 3.2.2.

3.3.2 Collision Time Prediction

The prediction of the future positions of the particles using Eq. (3.3.2) requires the time until the next discontinuity is reached by any pair of particles. This section outlines how these collision times are calculated.

For a hard sphere collision the distance between the particles must be equal to the collision diameter of the particles:

$$|\mathbf{r}_{ij} + \mathbf{v}_{ij}\Delta t| = \sigma \tag{3.3.3}$$

where $\mathbf{r}_{ij} = \mathbf{r}_i - \mathbf{r}_j$ is the separation vector between the two particles, while $\mathbf{v}_{ij} = \mathbf{v}_i - \mathbf{v}_j$ is the relative velocity of the particles. Equation (3.3.3) can be squared to give:

$$(\mathbf{r}_{ij} + \mathbf{v}_{ij}\Delta t)^2 = \sigma^2 \tag{3.3.4}$$

This is a quadratic equation for Δt and the solution is shown in Eq. (3.3.5).

$$\Delta t = \frac{(-\mathbf{v}_{ij} \cdot \mathbf{r}_{ij}) \pm \sqrt{(\mathbf{v}_{ij} \cdot \mathbf{r}_{ij})^2 - v_{ij}^2(r_{ij}^2 - \sigma^2)}}{v_{ij}^2} \tag{3.3.5}$$

There are two conditions that must be satisfied in order for a collision to occur. Firstly, the particles must be moving towards each other (i.e. Eq. (3.3.6a) must be true) and secondly, the roots of Eq. (3.3.5) must be real, therefore Eq. (3.3.6b) must apply. Physically this represents the condition that the particles must pass close enough to each other to collide.

$$\mathbf{v}_{ij} \cdot \mathbf{r}_{ij} < 0 \tag{3.3.6a}$$

$$(\mathbf{v}_{ij} \cdot \mathbf{r}_{ij})^2 - v_{ij}^2(r_{ij}^2 - \sigma^2) \geq 0 \tag{3.3.6b}$$

While there are two solutions to Eq. (3.3.5), only the earliest collision (the negative sign on the square root) needs to be considered. The second root gives the time when the particles would leave each other after they passed through one another, which cannot happen for hard spheres.

Since $\mathbf{v}_{ij} \cdot \mathbf{r}_{ij}$ must be negative for the collision, there is the possibility of catastrophic cancellation [9], if $(\mathbf{v}_{ij} \cdot \mathbf{r}_{ij})^2 \gg v_{ij}^2(r_{ij}^2 - \sigma^2)$. Therefore it is advisable to use the alternate form of the quadratic equation given in Eq. (3.3.7) [1].

$$\Delta t = \frac{r_{ij}^2 - \sigma^2}{(-\mathbf{v}_{ij} \cdot \mathbf{r}_{ij}) + \sqrt{(\mathbf{v}_{ij} \cdot \mathbf{r}_{ij})^2 - v_{ij}^2(r_{ij}^2 - \sigma^2)}} \tag{3.3.7}$$

When considering stepped potentials many of the same principles apply, except there are now two additional possible "collisions". The first, when two particles enter a step is treated identically to hard spheres. The other event, when the particles leave the step, is calculated using the second, later root of the quadratic. In order to prevent loss of numerical precision, the leaving time should be calculated using Eq. (3.3.8).

$$\Delta t = \frac{(-\mathbf{v}_{ij} \cdot \mathbf{r}_{ij}) + \sqrt{(\mathbf{v}_{ij} \cdot \mathbf{r}_{ij})^2 - v_{ij}^2(r_{ij}^2 - \sigma^2)}}{v_{ij}^2} \tag{3.3.8}$$

This allows the calculation of the time when a discontinuity occurs. The next section will discuss the technique used to solve the discontinuity itself.

3.3.3 Collision Dynamics

Once the time of the next collision is known, the particles can be moved to their new locations, using Eq. (3.3.2). However, in order to predict future collisions the post-collision velocities of the colliding particles must also be calculated.

The simplest collision between two particles is an elastic bounce, where the velocities and just exchanged along the separation vector between the two particles [2]. The change in velocity during the collision for particles i and j is given by: Eq. (3.3.9).

$$\Delta \mathbf{v}_i = -(\mathbf{v}_{ij} \cdot \hat{\mathbf{r}}_{ij})\hat{\mathbf{r}}_{ij} \tag{3.3.9a}$$

$$\Delta \mathbf{v}_j = (\mathbf{v}_{ij} \cdot \hat{\mathbf{r}}_{ij})\hat{\mathbf{r}}_{ij} \tag{3.3.9b}$$

For stepped potential system, the collision dynamics are more complex. When two particles collide they must pay an energy "cost" to proceed through the step. This energy cost, $\Delta\Phi$, is the difference in the energy of the current step and the step the particles are going into, and is shown in Eq. (3.3.10).

$$\Delta\Phi = \Phi_{\text{next step}} - \Phi_{\text{current step}} \tag{3.3.10}$$

If the kinetic energy of the particles is insufficient, the pair bounce off the step and the post-collision velocities are calculated using Eq. (3.3.9). However, if the particles have sufficient energy i.e. the inequality Eq. (3.3.11) is true, then the particles can enter the step.

$$\frac{1}{4}m(\mathbf{v}_{ij} \cdot \hat{\mathbf{r}}_{ij})^2 > \Delta\Phi \tag{3.3.11}$$

The change in the velocities of particles i and j after going through a step are shown in Eq. (3.3.12) where A is given in Eq. (3.3.13); the derivation of these equations is given in Appendix A. If the particles are entering a step, the positive square root of A is used, whereas if the particles are leaving a step it is the negative square root that should be used.

$$\Delta\mathbf{v}_i = \frac{A}{m}\hat{\mathbf{r}}_{ij} \tag{3.3.12a}$$

$$\Delta\mathbf{v}_j = -\frac{A}{m}\hat{\mathbf{r}}_{ij} \tag{3.3.12b}$$

$$A = -\frac{m}{2}\left((\mathbf{v}_{ij} \cdot \hat{\mathbf{r}}_{ij}) \pm \sqrt{(\mathbf{v}_{ij} \cdot \hat{\mathbf{r}}_{ij})^2 - \frac{4}{m}\Delta\Phi}\right) \tag{3.3.13}$$

It can be noticed that Eq. (3.3.9) can be derived from Eqs. (3.3.12) and (3.3.13) by setting $\Delta\Phi = 0$.

3.3.4 General Algorithm for Event-Driven Simulation

The algorithm used for the event-driven simulation is very similar to the algorithm used by Alder and Wainwright [10] and is shown below:

1. Initialisation.
2. Find the next event.
3. Process the event.
4. Update the event list.
5. Measure properties.
6. Repeat steps 2-5 for the desired number of events.

Several parts of this algorithm apply to both event and force-driven simulations are discussed in more depth in the following sections.

3.4 Initialisation

Both the force and even-driven simulators written for this dissertation initialise the particles in the same way. The particles are initially placed in a Face Centred Cubic

(FCC) structure. The use of the FCC lattice is common when simulating Lennard-Jones potentials as it is the closest possible packing of mono-sized spheres.

The particle velocities are then assigned randomly from a Gaussian distribution with a mean, $\mu = 0$, and a standard deviation, $\sigma = \sqrt{T^*}$, where T^* is the desired reduced temperature. The velocities are then rescaled to ensure there is no net shift in linear momentum in any direction by applying Eq. (3.4.1).

$$\mathbf{v}_i^{\text{new}} = \mathbf{v}_i^{\text{old}} - \frac{1}{N}\sum_{i}^{N} \mathbf{v}_i^{\text{old}} \tag{3.4.1}$$

3.5 Periodic Boundary Conditions

When simulating a system it is necessary to have a boundary to prevent the particles from moving away from each other into infinity. However solid walls have a large effect on the properties of a system so an alternative method is needed. Since the earliest MD simulations [10], periodic boundary conditions have been used to solve this problem.

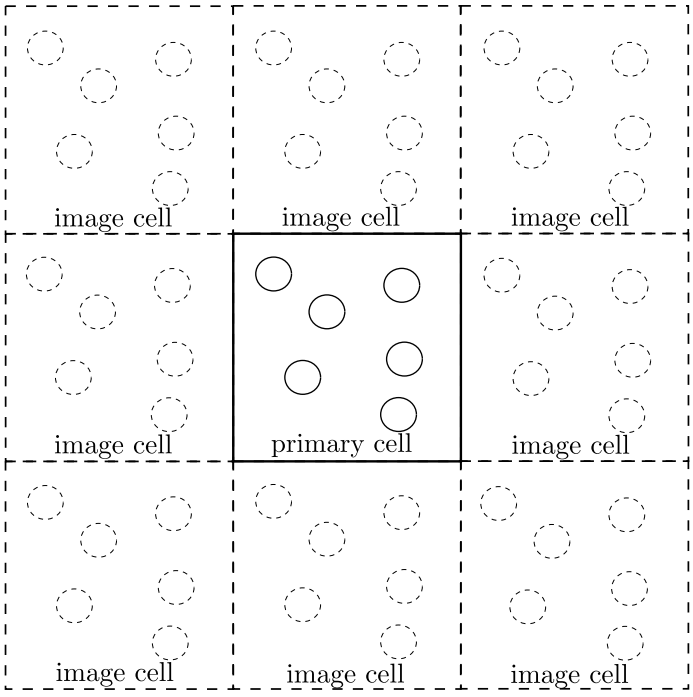

Figure 3.1: Figure showing 2D periodic boundary conditions. Only the nearest eight images (dashed) to the simulated system (solid) are shown.

The concept behind periodic boundary conditions is to create a pseudo-infinite system made up of tessellated images of the simulated system (as shown in Fig. 3.1). When a particle leaves the primary cell, its image enters from the opposite side. This ensures mass is conserved in each cell.

The problem with this is that particles can interact with multiple images of another particle. Molecular simulations use the minimum image criterion to ensure particles only interact with the closest image of another particle. In event-driven simulators only the collision time with the nearest image is considered, but this is not necessarily the same image as the one the particle will collide with next. The event-driven simulator in this dissertation recalculates the collision time if the particle has travelled far enough $(1/4(\text{box length} - \sigma))$ to collide with an image other than the nearest one.

3.6 Thermostat

All simulations in this dissertation use the canonical NVT ensemble, i.e. the number of particles, N, the volume of the system, V and the temperature, T were kept constant during the simulation. While keeping the number of particles and system size constant is simple, controlling the temperature is more complex.

The simplest method for controlling the temperature is to rescale the particle velocities to match the desired temperature using Eq. (3.6.1).

$$\mathbf{v}_{\text{new}} = \mathbf{v}_{\text{old}} \sqrt{\frac{T_{\text{desired}}}{T_{\text{current}}}} \tag{3.6.1}$$

However this does not allow energy fluctuations that should exist in a NVT system, therefore an Andersen thermostat [11] is used. An Andersen thermostat works by colliding a random particle with a ghost particle at the desired temperature. In this force-driven simulation, this is achieved by reassigning the velocities of 5% of particles from a Gaussian distribution at the correct temperature (similar to Sec. 3.4) on every time-step.

For the event-driven simulation a more sophisticated implementation is used. An extra event is created for the thermostat, with the time to the event calculated from an exponential distribution with a rate of 20 thermostat events per unit time. The reason an exponential distribution is used is that the thermostat is an example of a Poisson Process, where an event happens at a constant rate yet each event occurs independently. At this thermostat event a random particle has its velocities reassigned from the Gaussian distribution at the desired temperature, similar to the force-driven simulation.

3.7 Optimisation

Due to the time-consuming nature of computer simulations there are a number of techniques used to reduce their running times. This section will outline a number of the techniques implemented in the programs coded for this dissertation.

3.7.1 Truncation of the Potential

Since the calculation of the forces on the particles is the most time-consuming part of force-driven simulations [12], almost all optimising techniques focus on this aspect.

A simple yet effect technique to improve simulation speed is to truncate the potential. Since continuous potentials tend to zero as particles get further away from each other, significant time can be saved by selecting a cut-off radius at which the potential is taken to be zero. The form of a truncated potential is shown in Eq. (3.7.1). For the Lennard-Jones potential a cut-off radius of 3σ is used as $\Phi(3\sigma) = -0.00548\varepsilon$ and $F(3\sigma) = -0.0109\varepsilon/\sigma$ are both approximately 0.5% of the minimum energy or maximum attractive force respectively.

$$\Phi(r) = \begin{cases} \Phi(r) & \text{if } r \leq r_{\text{cut-off}} \\ 0 & \text{if } r > r_{\text{cut-off}} \end{cases} \tag{3.7.1}$$

3.7.2 Neighbour Lists

While truncating the potential prevents the calculation of the forces it still requires the computation of the distance between particles. These extraneous calculations can be eliminated by using a neighbour list.

There are two main types of neighbour list used in molecular dynamics simulations. The first is the use of Verlet lists [3], and this is the type used in this dissertation for the force-driven simulation. A Verlet list is a list of all the particles within a certain radius of a particle. If this list was updated every time-step, this would be no improvement on the original method, but by making the Verlet radius larger than the truncation radius, this list can be used for multiple time-steps. Haile [2] recommends using a Verlet radius of 3.3σ, and updating the list every 10 time-steps, and this is what was done in this dissertation for the force-driven simulator.

Another method is to use cell-linked lists [1], which involves dividing the system into a grid and only the particles in the same cell or a neighbouring cell are taken into account. This method can be inefficient as the length of each cell must be at least the truncation cut-off radius wide to prevent particles being missed out. This means a volume of $27r^3_{\text{cut-off}}$ (as in 3 dimensions each cell has 26 neighbours) are considered but only particles within the spherical volume $\frac{4}{3}\pi r^3_{\text{cut-off}}$ should be checked; this means the volume tested is over six times larger than it needs to be.

Mattson and Rice [13] improve this by reducing the length of each cell to less than the cut-off radius, but this results in more neighbouring cells having to be checked i.e. for a cell length of $0.5r_{\text{cut-off}}$ the nearest 124 (a $5 \times 5 \times 5$ grid) cells are considered neighbours. This means there is a compromise as smaller cells mean that less volume is checked, but also means the cell lists are made obsolete quicker and therefore have to generated more

frequently.

Neighbour lists can be implemented in event-driven simulators as well, and are of the cell-linked list type as this best utilises the event-driven nature of these simulators. However due to time constraints one was not implemented in the event-driven simulator used for this dissertation.

3.7.3 Optimisation for Event-Driven Simulators

Although no neighbour list was implemented in the event-driven simulator a number of other optimisation techniques were used. Due to the more complex nature of event-driven simulations there are a larger number of methods used to increase simulator efficiency. Whereas in the force-driven simulator the calculation of the forces was the most time-consuming part, in event-driven simulators it is calculation of the collision time that is the most computationally intensive.

When two particles collide, only the velocities of those two particles change. This means that the collision times for every collision that did not involve either of the two particles is still valid. Rather than recalculating these collision times every cycle, they are stored in an event list and are only updated when they change.

The inclusion of an event list means it must be sorted to find the earliest event. The time taken to sort the event list increases with the number of events therefore it is desired to have as short a list as possible (there are examples of $\mathcal{O}(1)$ priority queues that do not have this problem [14]). Therefore every particle has its own event list and only the earliest event of each particle is stored in the master event list. The event list used in this dissertation was not fully sorted, it was only searched for the earliest event.

However when two particles collide their events with every other particle become obsolete, but these events are spread over every particles' individual event list. The time spend searching for and deleting these obsolete events can be saved by only updating them when they reach the top of the event list. A parameter such as the number of collisions the particles have undergone is used to decide whether an event is valid and can be executed or obsolete and needs to be updated [1].

These optimisation techniques can increase the speed of a simulation by an order of magnitude or more and allow larger systems of particles to be simulated for longer periods of time which ensures accuracy of the results obtained in this dissertation.

3.8 Summary

The outlines for the algorithms for event-driven and force-driven simulators have been given in this chapter. Force-driven simulators are much more popular due to their simplicity but their solution is only approximate and is subject to large numerical errors.

Event-driven simulators do not have these same errors but they are significantly more complex. This is highlighted in that over 2200 lines of code are required for the event-driven simulator whereas the force-driven simulator needs less than 1000 to simulate the same system.

While event-driven simulators are more accurate, and hence more desirable, all the sophisticated potentials in the literature are continuous. This means that force-driven simulators must be used to simulate these models. The aim of this dissertation is to bridge the gap between these two classes of potentials and this will be discussed in Chap. 5. In the following chapter the methods used to measure some of the properties of molecular systems so the results from continuous and discontinuous models can be compared.

3.9 References

[1] Pöschel, T.; Schwager, T., *Computational Granular Dynamics: Models and Algorithms*; Springer: 2005.

[2] Haile, J. M., *Molecular Dynamics Simulation: Elementary Methods*; Wiley-Interscience: 1997.

[3] Verlet, L. Computer "Experiments" on Classical Fluids. I. Thermodynamical Properties of Lennard-Jones Molecules. *Phys. Rev.* **1967**, *159*, 98–103, DOI: 10.1103/PhysRev.159.98.

[4] Gear, C. W., *Numerical Initial Value Problems in Ordinary Differential Equations*; Forsythe, G., Ed.; Prentice-Hall: 1971.

[5] Hairer, E.; Lubich, C.; Wanner, G. Geometric Numerical Integration Illustrated by the Stormer-Verlet Method. *Acta Numerica* **2003**, *12*, 399–450, DOI: 10.1017/S0962492902000144.

[6] Swope, W. C.; Andersen, H. C.; Berens, P. B.; Wilson, K. R. A Computer Simulation Method for the Calculation of Equilibrium Contants for the Formation of Physical Clusters of Molecules: Application to Small Water Clusters. *J. Chem. Phys.* **1982**, *76*, 637–649, DOI: 10.1063/1.442716.

[7] Khakimov, Z. New Integrator for Molecular Dynamics Simulations. *Comput. Phys. Commun.* **2002**, *147*, 733–736, DOI: 10.1016/S0010-4655(02)00387-9.

[8] Rahman, A Correlations in the Motion of Atoms in Liquid Argon. *Phys. Rev.* **1964**, *136*, A405–A411, DOI: 10.1103/PhysRev.136.A405.

[9] Goldberg, D. What Every Computer Scientist Should Know About Floating-Point Arithmetic. *ACM Comput. Surv.* **1991**, *23*, 5–48, DOI: 10.1145/103162.103163.

[10] Alder, B. J.; Wainwright, T. E. Studies in Molecular Dynamics. I. General Method. *J. Chem. Phys.* **1959**, *31*, 459–466, DOI: 10.1063/1.1730376.

[11] Andersen, H. C. Molecular Dynamics Simulations at Constant Pressure and/or Temperature. *J. Chem. Phys.* **1980**, *72*, 2384–2393, DOI: 10.1063/1.439486.

[12] Frenkel, D.; Smit, B., *Understanding Molecular Simulations*, 2nd Edition; Academic Press: 2002, DOI: 10.1016/B978-012267351-1/50006-7.

[13] Mattson, W.; Rice, B. M. Near-Neighbour Calculations using a Modified Cell-Linked List Method. *Comput. Phys. Commun.* **1999**, *119*, 135–148, DOI: 10.1016/S0010-4655(98)00203-3.

[14] Paul, G. A Complexity O(1) Priority Queue for Event Driven Molecular Dynamics Simulations. *J. Comput. Phys.* **2007**, *221*, 615–625, DOI: 10.1016/j.jcp.2006.06.042.

CHAPTER

FOUR

MEASURING THERMODYNAMIC PROPERTIES

Until now only the motion of the system has been calculated, but the positions and velocities are only the means to an end. The real purpose of a molecular dynamics simulation is to the measure thermodynamic properties of the system. First, the need for time averaging of these properties is discussed, and this is followed by a description of the techniques used to measure various properties (energy, temperature, pressure, radial distribution function). Finally, the system of units commonly used in molecular dynamics, and the system used in this dissertation is discussed.

4.1 Time Averaging

Molecular dynamics is a useful tool to predict macroscopic properties of molecular systems. However, even when the system is at equilibrium, the values of these properties fluctuate around a mean (see Fig. 4.1) therefore it is common to take time averages of these values. These time averages are denoted with angle brackets $\langle\ \rangle$, and the time average of a property, A, is shown in Eq. (4.1.1) [1].

$$\langle A \rangle = \lim_{t\to\infty} \frac{1}{t} \int_{t_0}^{t_0+t} A(\tau)\mathrm{d}\tau \tag{4.1.1}$$

This time average can be calculated precisely in event-driven simulations for several properties such as pressure, kinetic energy and potential energy. These only change at collisions and therefore are constant for the time between the collision and can be calculated using:

$$\langle A \rangle = \frac{1}{t} \sum^{N_{\text{coll}}} A(t_c)\Delta t \tag{4.1.2}$$

where N_{coll} is the number of collisions in time, t, and Δt is the time between the collision at time t_c and the next collision.

In force-driven simulators all properties change continuously and hence time averages cannot be calculated precisely, however approximations can be made. If properties are

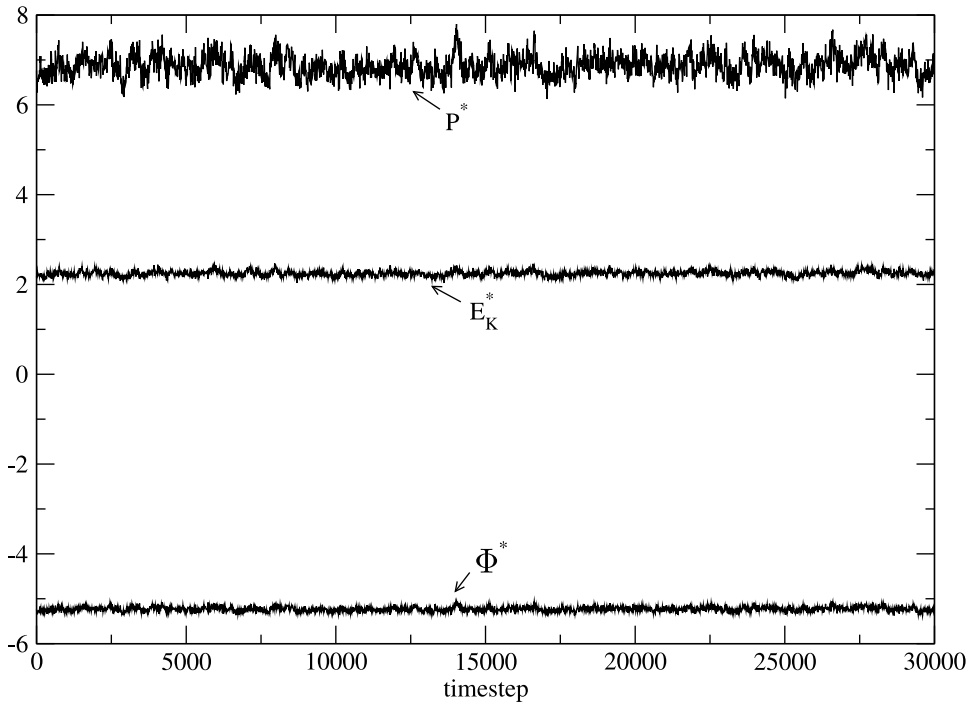

Figure 4.1: Plot showing fluctuation of pressure ($P^* = P\sigma^3/\varepsilon$), kinetic energy per particle ($E_K^* = E_K/N\varepsilon$) and potential energy per particle ($\Phi^* = U/N\varepsilon$). Results are from a force-driven simulation involving 864 particles, at a density $\rho^* = 0.9$ and temperature $\langle T^* \rangle = 1.497$. Values were collected every 10 time-steps where each time-step was $\Delta t^* = 0.005$.

measured every uniform period of time, the time average can be approximated by:

$$\langle A \rangle = \frac{1}{M} \sum_{1}^{M} A(\tau) \tag{4.1.3}$$

where M is the number of measurements taken.

4.2 Energy

Perhaps one of the most important properties to measure in MD simulations is the total internal energy of the system. For isolated systems, i.e. systems where mass or energy cannot enter or leave the system, this internal energy is the sum of kinetic and potential energy (Eq. (4.2.1)).

$$U = E_K + \Phi \tag{4.2.1}$$

The total kinetic energy in the system is the sum of the kinetic energy of each particle, as shown in Eq. (4.2.2).

$$E_K = \sum_{i}^{N} m v_i^2 \tag{4.2.2}$$

The potential energy of the system is the sum of the potential energy between every pair of particles (for a pairwise potential), and is shown in Eq. (4.2.3).

$$\Phi = \sum_{i} \sum_{<j} \Phi(r_{ij}) \tag{4.2.3}$$

Event-driven simulators strictly conserve energy, therefore the kinetic and potential energy can be measured at the beginning of the simulation and then updated whenever either changes e.g. when a collision occurs.

4.3 Temperature

The velocity distribution of particles is given by the Maxwell distribution [1]:

$$f(v_x)dv_x = \sqrt{\frac{m}{2\pi k_B T}} e^{-\frac{m v_x^2}{2 k_B T}} \tag{4.3.1}$$

where k_B is the Boltzmann Constant. This is the form of a Gaussian distribution and it can be shown [2] that the mean square velocity in any direction is as shown in Eq. (4.3.2).

$$\bar{v}_x^2 = \frac{k_B T}{m} \tag{4.3.2}$$

Making the assumption that the velocity distribution is the same in each direction (which is valid if the system is in equilibrium), the temperature can be expressed as Eq. (4.3.3), by taking the average temperature in each direction.

$$T^* = k_B T = \frac{m v^2}{3N} = \frac{2}{3N} E_K \tag{4.3.3}$$

This allows the calculation of the temperature from the kinetic energy of the system.

4.4 Pressure

The pressure in a molecular dynamics simulation is calculated using the virial equation of state (Eq. (4.4.1)) [2].

$$\frac{PV}{N k_B T} = 1 + B_2 \rho + B_3 \rho^2 + B_4 \rho^3 + ... \tag{4.4.1}$$

The coefficients, $B_2, B_3, B_4, ...$ are known as the second, third, fourth, etc. virial coefficients. Values for these virial coefficients are available in the literature for common potentials such as hard spheres [3] or Lennard-Jones [4]. Physically these coefficients represent the contribution to the pressure from the interaction of a particle with two, three, four, etc. other particles.

The second virial can be calculated using Eq. (4.4.2) [5] in three dimensions. Similar expressions can be written for the higher virial coefficients however the solution to these is very time-consuming.

$$B_2 = -2\pi \int_0^\infty \left(e^{\Phi(r)/k_B T} - 1\right) r^2 \mathrm{d}r \tag{4.4.2}$$

Therefore an alternative expression to measure the contribution to the pressure of all the virial coefficients has been created for both simulation methods by using kinetic theory and measuring momentum flux during the simulation. In force-driven simulations, the second virial can be calculated using Eq. (4.4.3) [1].

$$\frac{PV}{Nk_BT} = 1 + \frac{1}{3NkT} \left\langle \sum_{i<j} \sum \mathbf{F}_{ij} \cdot \mathbf{r}_{ij} \right\rangle \tag{4.4.3}$$

Calculating the pressure in event-driven simulators is more complex due to the lack of forces in the simulation, however by keeping track of the momentum flux at each collision an average pressure can be calculated using Eq. (4.4.4) [6]. Here N_{coll} is the total number of collisions during the time t.

$$\frac{PV}{Nk_BT} = 1 + \frac{m}{3} \frac{N_{\text{coll}}}{Nt} \langle \mathbf{r}_{ij} \cdot \Delta \mathbf{v}_i \rangle_{\text{coll}} \tag{4.4.4}$$

4.5 Radial Distribution Function

One of the most important measurements in molecular dynamics is the radial distribution function (RDF). The RDF provides information concerning the arrangement of the particles, and can be determined experimentally [7]. This means that the RDF can be used to determine the agreement of MD simulations and experimental results.

Statistically, the RDF is the ratio of the probability of finding a particle a distance r from another particle to the expected probability if the particles were randomly distributed [8]. Since potentials usually have a hard core there is very little chance of finding a particle within the radius of another particle, therefore the RDF is zero very close to the particle. However, as the radial distance tends to infinity the probability of finding a particle tends to the randomly distributed probability so the RDF tends to one, which can be seen in Fig. 4.2.

The RDF is measured in MD simulations by splitting the radial distance into a number

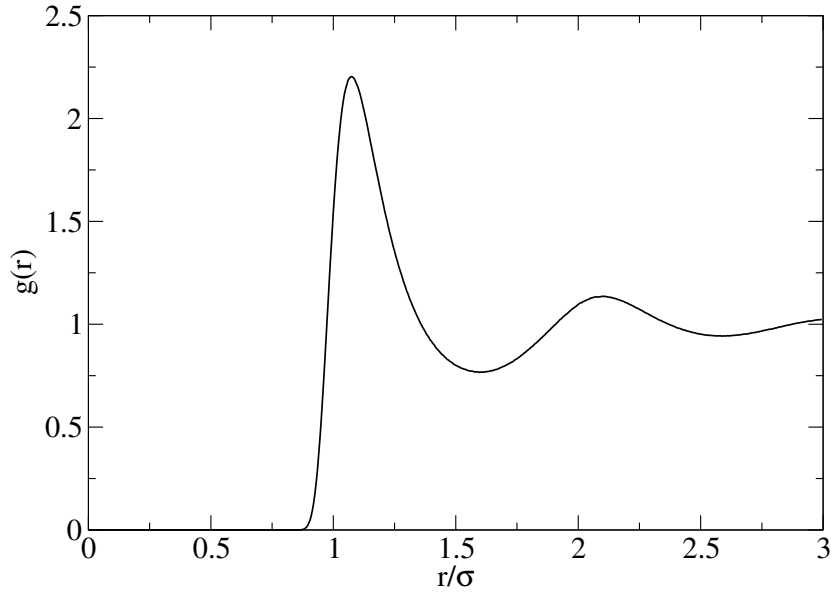

Figure 4.2: Plot of the radial distribution function, $g(r)$, for a continuous Lennard-Jones potential. Results taken from a force-driven simulation at $\rho^* = 0.7$ and $T^* = 1.5$.

of bins. The number of pairs of particles in a particular bin is then counted. The value of the RDF for bin n can be calculated using the following equation:

$$g(n) = \frac{N_n}{NV_{\text{bin}}\rho} \tag{4.5.1}$$

where V_{bin} is the volume of the bin, and N_n is the number of particle pairs in bin n. This measurement illustrates another definition of the RDF. The radial distribution function is the ratio between the density at a specific distance from another particle to the average density of the system.

Since the RDF contains information about the potential, simulations with discrete potentials produce radial distribution functions with discontinuities in them. Fig. 4.3 shows the RDF produced when using the stepped potential shown in Fig. 2.5.

This discontinuous RDF can be converted to a continuous function by using the indirect correlation function, $y(r)$, [9]. The indirect correlation function can be defined for both continuous and discontinuous RDF and potentials using:

$$y(r) = g_d(r)e^{\beta\Phi_d(r)} = g_c(r)e^{\beta\Phi_c(r)} \tag{4.5.2}$$

where $\beta = 1/k_BT$ and the subscripts c and d denote the continuous and discontinuous functions respectively. The continuous form of the RDF can then be calculated using Eq. (4.5.3). Fig. 4.4 shows the continuous form of the discontinuous RDF shown in Fig. 4.3.

$$g_c(r) = g_d(r)e^{[\Phi_d(r)-\Phi_c(r)]\beta} \tag{4.5.3}$$

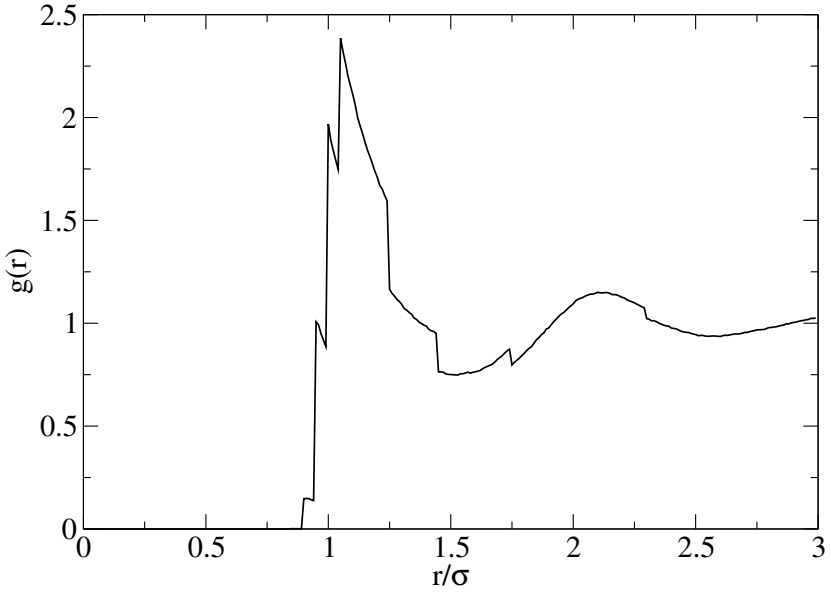

Figure 4.3: Plot of the radial distribution function, $g(r)$, for a discrete stepped potential. Results taken from a event-driven simulation at $\rho^* = 0.7$ and $T^* = 1.5$.

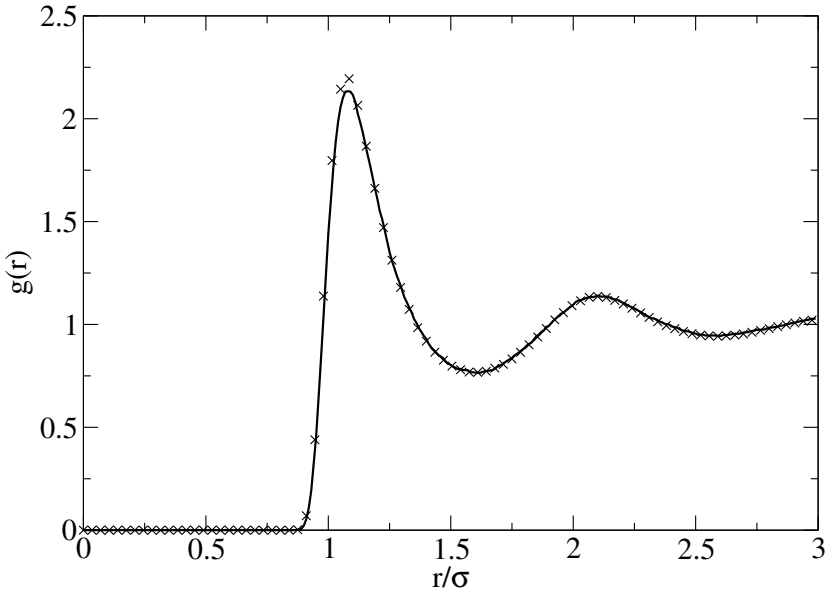

Figure 4.4: The continuous form of the radial distribution function of a discrete potential is shown with the solid line. The crosses show the RDF obtained from the continuous Lennard-Jones potential. Both were obtained at $\rho^* = 0.7$ and $T^* = 1.5$.

4.6 Measuring Properties using the Radial Distribution Function

Another reason why the radial distribution functions is so important is that it can be used to calculate other thermodynamic properties. Any pair function can be related to the RDF [8], but the two most important are the potential energy and the pressure, which can be related to the RDF using Eqs. (4.6.1) and (4.6.2) respectively.

$$\Phi = 2\pi\rho N \int_0^\infty \Phi(r) g(r) r^2 \mathrm{d}r \tag{4.6.1}$$

$$P = \rho k_B T + \frac{2\pi}{3}\rho^2 \int_0^\infty r F(r) g(r) r^2 \mathrm{d}r \tag{4.6.2}$$

However, in MD simulations these properties are usually measured using the methods discussed in Secs. 4.2 and 4.4 as these are usually more accurate.

4.7 Long-Range Corrections

In Sec. 3.7, the truncation of the potential to increase simulator performance was discussed. While particles far apart exert little force between each other, the contributions to the thermodynamic properties can still be significant. Therefore it is common in MD simulations to account for the truncated potential by adding on a long-range correction.

These long range corrections can be calculated using Eqs. (4.6.1) and (4.6.2). Since the RDF tends to one as separation distance tends to infinity, $g(r)$ is assumed to be one in these corrections. Similarly since the potential, $\Phi(r)$, and the force, $F(r)$, tend to zero as r increases, these are assumed to be zero. Making these assumptions and by splitting the integrals Eqs. (4.6.1) and (4.6.2) can be integrated to give equations:

$$\Phi = \Phi_{\text{MD}} + \frac{8\pi\rho}{3r_c^3}\left(\frac{1}{3r_c^6} - 1\right) \tag{4.7.1}$$

$$P = P_{\text{MD}} + \frac{16\pi\rho^2}{3r_c^3}\left(\frac{2}{3r_c^6} - 1\right) \tag{4.7.2}$$

where r_c is the truncation radius of the potential, and the subscript MD denotes the property measurement from the MD simulation. These give the long-range corrections for the potential energy and the pressure respectively.

4.8 Units

In molecular dynamics simulations, properties are frequently measured in dimensionless forms [1]. These "reduced units" are usually denoted with an asterisk. In order to achieve this a number of fundamental dimensions are needed: a characteristic length σ, a characteristic energy ε, and the mass of one particle m. In the case of the Lennard-Jones potential, the characteristic length and energy are taken as the distance of the root, and the depth of the attractive well respectively. A list of reduced forms are given in Table 4.1.

Table 4.1: Table of reduced forms of various quantities used in this dissertation [1].

Quantity	Reduced forms
Density	$\rho^* = N\sigma^3/V$
Energy	$U^* = U/\varepsilon$
Force	$F^* = F\sigma/\varepsilon$
Length	$r^* = r/\sigma$
Pressure	$P^* = P\sigma^3/\varepsilon$
Temperature	$T^* = kT/\varepsilon$
Time	$t^* = t/(\sigma\sqrt{m/\varepsilon})$
Velocity	$v^* = v\sqrt{m/\varepsilon}$

4.9 References

[1] Haile, J. M., *Molecular Dynamics Simulation: Elementary Methods*; Wiley-Interscience: 1997.

[2] Landau, L.; Lifshitz, E., *Statistical Mechanics*, 2nd; Course of Theoretical Physics, Vol. 5; Pergamon: Oxford, 1968.

[3] Labík, S.; Kolafa, J.; Malijevský, A. Virial Coefficients of Hard Spheres and Hard Disks up to the Ninth. *Phys. Rev. E* **2005**, *71*, 021105, DOI: 10.1103/PhysRevE.71.021105.

[4] Schultz, A. J.; Kofke, D. A. Sixth, Seventh and Eighth Virial Coefficients of the Lennard-Jones Model. *Mol. Phys.* **2009**, *1007*, 2309–2318, DOI: 10.1080/00268970903267053.

[5] Smith, J. M.; Van Ness, H. C.; Abbott, M., *Introduction ot Chemical Engineering Thermodynamics*, 7th; McGraw-Hill: New York, 2005.

[6] Lue, L. Collision Statistics, Thermodynamics, and Transport Coeffiecients of Hard Hyperspheres in Three, Four, and Five Dimensions. *J. Chem. Phys.* **2005**, *122*, 044513, DOI: 10.1063/1.1834498.

[7] Yarnell, J. L.; Katz, M. J.; Wenzel, R. G. Structure Factor and Radial Distribution Function for Liquid Argon at 85 °K. *Phys. Rev. A* **1973**, *7*, 2130–2144, DOI: 10.1103/PhysRevA.7.2130.

[8] Allen, M.; Tildesley, D. J., *Computer Simulation of Liquids*; Oxford University Press: 1987.

[9] Chapela, G.; Scriven, L. E.; Davis, H. T. Molecular Dynamics for Discontinuous Potential. IV. Lennard-Jonesium. *J. Chem. Phys.* **1989**, *91*, 4307, DOI: 10.1063/1.456811.

CHAPTER

FIVE

CONVERTING CONTINUOUS POTENTIALS TO DISCRETE POTENTIALS

In the previous chapters the tools required to test the effectiveness of a potential conversion algorithm were discussed. This chapter will describe the methods for converting continuous to discrete potentials that were tried in this

5.1 Introduction

Discontinuous potentials have a number of desirable properties. Due to the analytical nature of event-driven simulation (see Sec. 3.3.1), discontinuous potentials can be solved precisely, eliminating the errors and instability inherent to integrators. It is also possible to theoretically derive the equation of state for a discrete potential fluid using thermodynamic perturbation theory.

There is, however, a major problem that limits the impact discrete potentials have had to molecular dynamics. Firstly, event-driven simulators are significantly more complex to implement which reduces the usage of discrete potentials in the literature. This means while there are many advanced continuous potentials available, discrete potentials still remain relatively basic.

If a general method to convert continuous potentials to equivalent discrete potentials could be developed this would allow the large number of continuous potentials in the literature to be incorporated into discrete molecular dynamics.

There are two parameters that need to be decided in order to create a stepped potential: the placement of the steps; and the energy (or height) of the steps. The setting of these parameters will be discussed in the following sections

5.2 Setting Step Positions

5.2.1 Stepping in Even Probability

The first method that was tried was to step in equal probabilities of a particle being at a certain location. This should mean there are more steps at locations where there are more particles. Setting step positions in probability is equivalent to setting steps in even values of the partition function. The partition function [1] for a pair of particles is given by:

$$Z(r_n, r_{n+1}) = 4\pi \int_{r_n}^{r_{n+1}} e^{-\beta\Phi(r)} r^2 \mathrm{d}r \tag{5.2.1}$$

where, r_n denotes the position of the n^{th} step and $\beta = 1/T^*$. By starting at $r_1 = r_{\text{core}}$ the position of the other steps can be found by solving:

$$Z(r_n, r_{n+1}) = \frac{Z(r_{\text{core}}, r_{\text{cutoff}})}{N_s} \tag{5.2.2}$$

for r_{n+1} over the number of steps, N_s, until $r_{n+1} = r_{\text{cutoff}}$. The solution to Eq. (5.2.2) is problematic as the variable is a limit of an integral. This was solved using a bisection method while the integral was calculated using Simpson's Rule.

5.2.2 Stepping in the Magnitude of the Expected Force

Though stepping in even probability makes some sense, it makes the invalid assumption that particles at any position make the same contribution to system properties. This is not the case as particles close together experience a higher force and hence make significant contributions to the pressure and potential energy of the system. Therefore the stepping method must taken into account not just the number of particles but some measure of the effect, such as the force. The problem with using the force is that can be both positive or negative which makes stepping in equal values of it impractical. Therefore the magnitude of the force is used to create Eq. (5.2.3).

$$F_E(r_n, r_{n+1}) = 4\pi \int_{r_n}^{r_{n+1}} |F(r)| e^{-\beta\Phi(r)} r^2 \mathrm{d}r \tag{5.2.3}$$

Stepping in equal values of Eq. (5.2.3) is achieved in a similar manner to even probability in the preceding section using Eq. (5.2.4).

$$F_E(r_n, r_{n+1}) = \frac{F_E(r_{\text{core}}, r_{\text{cutoff}})}{N_s} \tag{5.2.4}$$

5.2.3 Setting the Position of the Hard Core

Neither of the two above methods set a suitable location for a hard core. All stepped potentials need a hard core to prevent particles from entering each other, where there is no force to push them apart.

A two methods are considered to define r_{core}. The first is to use the Barker-Henderson equivalent hard sphere diameter [2]:

$$r_{\text{core}} = \int_0^{\sigma} \left(1 - e^{\beta\Phi(r)}\right) \mathrm{d}r \tag{5.2.5}$$

The second is to place the core where there is a very low probability of particles getting there. This can be done using the partition function similar to Sec. 5.2.1 using:

$$Z(0, r_{\text{core}}) = P_{\text{core}} Z(0, r_{\text{cutoff}}) \tag{5.2.6}$$

where P_{core} is the desired probability of particles reaching the core.

Now that the methods for setting the positions of the steps, the next section will describe the methods for setting the heights of the steps.

5.3 Setting Step Energies

5.3.1 Setting Heights to Fix Probabilities

The heights of the steps can be set to ensure the partition function is the same for both continuous and discrete potentials. Equation (5.2.1) can be integrated over a discrete step to give:

$$Z(r_n, r_{n+1}) = \frac{4\pi}{3} \left(r_{n+1}^3 - r_n^3\right) e^{-\beta\Phi_n} \tag{5.3.1}$$

where Φ_n is the height of the step, n, that lies from $r_n \to r_{n+1}$. This must be equal to the continuous partition function therefore by equating Eqs. (5.2.1) and 5.3.1 an expression can be created for the height of a single step (Eq. (5.3.2)).

$$\Phi_n = -\beta^{-1} \ln \left(\frac{3}{r_{n+1}^3 - r_n^3} \int_{r_n}^{r_{n+1}} e^{-\beta\,\Phi(r)}\, r^2 \mathrm{d}r \right) \tag{5.3.2}$$

Setting the step energies to ensure agreement between the probabilities of both continuous and discrete potentials should also ensure that the second virial coefficient is the same. If a similar series of steps as above were to be carried out on Eq. (5.3.3) an identical result to Eq. (5.3.2) would be obtained.

$$B_2(r_n, r_{n+1}) = -2\,\pi \int_{r_n}^{r_{n+1}} \left(e^{-\beta\,\Phi(r)} - 1\right) r^2 \mathrm{d}r \tag{5.3.3}$$

5.3.2 Setting Heights to Fix Potential Energy

The expected value for the potential energy between two particles is the probability of a particle multiplied by the potential energy integrated over the position. This means that the expected potential energy is given by:

$$\langle \Phi \rangle_{r_n}^{r_{n+1}} = 4\,\pi\, Z^{-1}(r_n, r_{n+1}) \int_{r_n}^{r_{n+1}} \Phi(r) e^{-\beta\Phi(r)} r^2 \mathrm{d}r \tag{5.3.4}$$

This expected energy over a single discrete step is simply the energy of the step. This allows the setting of the heights to ensure the potential energy of the system is the same in both continuous and discrete.

A number of techniques to create a general method to convert between continuous and discrete potentials have been outlined in this section. It should be noted that many of the expressions in this chapter make the assumption that the RDF, $g(r) = 1$. This is necessary to derive these equations but is a strictly invalid assumption. In the next chapter these techniques are tested and compared to continuous potential results to investigate which combination of techniques produces the most similar stepped potential.

5.4 References

[1] Landau, L.; Lifshitz, E., *Statistical Mechanics*, 2nd; Course of Theoretical Physics, Vol. 5; Pergamon: Oxford, 1968.

[2] Barker, J. A.; Henderson, D. Perturbation Theory and Equation of State for Fluids: II. A Successful Theory of Liquids. *J. Chem. Phys.* **1967**, *47*, 4714–4721.

CHAPTER

SIX

RESULTS AND DISCUSSION

All the tools and techniques needed to compare a discrete and continuous potential have been discussed. In this chapter, the simulators created for this work will be validated against other simulators and literature values to ensure that they function correctly. Then, all the stepping techniques described in the previous section will be tested and the best methods will be combined to produced a general stepping method. Finally, steps produced by this method will be compared to the steps obtained by Chapela *et al.* [1].

6.1 Benchmarking

6.1.1 Force-Driven Simulator

The results from the force-driven simulation were checked against a publicly available force-driven simulation, called ESPResSo [2]. Simulations were run at $T^* = 1.5$ for 50000 time-steps using 864 particles. Measurements were taken every 10 time-steps for the last 30000 steps of the simulation. The mean and standard deviations of the results of ten simulation runs are shown in Table 6.1. Very good agreement is shown between all values with deviations falling inside standard deviations.

6.1.2 Event-Driven Simulator

Due to the complex nature of event-driven simulations the benchmarking was split into two tests.

Testing Hard Spheres

The event-driven simulator was first tested running a hard sphere simulation before testing the more complex stepped potentials. A single 'step' with a energy requirement sufficiently large such that no particle could enter it. The simulation was run once at a range of densities using 864 particles at a reduced temperature of $T^* = 1$ for 5 million collisions,

Table 6.1: Comparison of results obtained by the force-driven simulator coded for this dissertation and the publicly available simulator, ESPResSo. The numbers in brackets show the standard deviation in the last digit.

ρ^*	$\langle T^* \rangle$		$\langle P^* \rangle$		$\langle \Phi^* \rangle$	
	Simulator	ESPResSo	Simulator	ESPResSo	Simulator	ESPResSo
0.1	1.499(2)	1.500(4)	0.1224(3)	0.1227(5)	-0.708(3)	-0.705(2)
0.2	1.499(2)	1.500(4)	0.2069(7)	0.207(1)	-1.360(9)	-1.366(5)
0.3	1.499(2)	1.501(2)	0.280(1)	0.282(2)	-1.975(5)	-1.979(5)
0.4	1.499(1)	1.500(2)	0.379(4)	0.377(3)	-2.568(5)	-2.569(3)
0.5	1.499(2)	1.500(3)	0.567(5)	0.568(5)	-3.164(3)	-3.165(3)
0.6	1.500(2)	1.500(4)	0.988(6)	0.988(9)	-3.771(1)	-3.774(2)
0.7	1.499(1)	1.501(3)	1.894(5)	1.90(1)	-4.358(2)	-4.360(2)
0.8	1.499(2)	1.498(2)	3.68(1)	3.68(1)	-4.869(2)	-4.872(2)
0.9	1.499(1)	1.501(3)	6.88(1)	6.90(2)	-5.227(2)	-5.226(4)

the results were compared with those of Lue [3] in Table 6.2. The agreement between results is good and lies within statistical uncertainty. The largest discrepancies are in the values for the coefficient of diffusion at low densities which is probably due to Lue's values were obtained after 10 million collisions which is longer than the 5 million collisions run by the event-driven simulator.

Table 6.2: Comparison of results obtained by the event-driven simulator with literature values. t_{avg} is the average time between collisions, $\langle \hat{\mathbf{r}} \cdot \Delta \mathbf{v} \rangle_{coll}$ is the average momentum transfer per collision, and D is the coefficient of diffusion.

ρ	t_{avg}		$\langle \hat{\mathbf{r}} \cdot \Delta \mathbf{v} \rangle_{coll}$		D	
	Simulator	Lue	Simulator	Lue	Simulator	Lue
0.3	0.3052	0.3052	1.775	1.772	0.53	0.55
0.4	0.1944	0.1942	1.776	1.773	0.341	0.359
0.5	0.13024	0.13031	1.774	1.7724	0.247	0.247
0.6	0.08966	0.08968	1.771	1.7721	0.169	0.173
0.7	0.0625	0.0625	1.773	1.776	0.114	0.113
0.8	0.04365	0.0436	1.772	1.772	0.064	0.065
0.9	0.03029	0.03024	1.773	1.772	0.033	0.0327

Testing Step Potentials

The simulator was then benchmarked using a step potential. The results were compared with Chapela *et al.* [1] using their 'Case 6' steps. The simulation was run for 1.5 million collisions using 864 particles. Each simulation was run ten times and the mean values and standard deviations are given in Table 6.3.

Table 6.3: Comparison of results obtained by the event-driven simulator with literature values using stepped potentials. Numbers in parenthesis indicate the standard deviation in the final digit.

ρ	$\langle T \rangle$		$\langle U \rangle$		$\langle P \rangle$	
	Simulator	Chapela *et al.*	Simulator	Chapela *et al.*	Simulator	Chapela *et al.*
0.85	0.719(3)	0.72	-6.04(7)	-5.80	-0.5(4)	0.54
0.85	1.339(8)	1.34	-5.130(9)	-5.14	4.08(4)	4.08
0.85	2.35(1)	2.35	-4.24(2)	-4.20	8.78(9)	8.86
0.85	3.37(2)	3.37	-3.48(2)	-3.49	12.90(9)	13.00
0.85	4.59(1)	4.60	-2.67(1)	-2.68	17.31(8)	13.43
0.75	0.811(2)	0.81	-5.095(3)	-5.08	-0.20(2)	-0.24
0.75	1.309(9)	1.31	-4.67(1)	-4.63	1.81(5)	1.84
0.75	2.49(1)	2.49	-3.88(1)	-3.82	5.80(4)	5.95
0.75	3.59(2)	3.59	-3.26(1)	-3.22	9.03(7)	9.20
0.65	1.309(8)	1.31	-4.081(8)	-4.06	0.80(3)	0.81
0.65	2.61(1)	2.61	-3.42(1)	-3.41	3.86(5)	3.89
0.65	3.79(1)	3.79	-2.926(9)	-2.94	6.34(7)	6.33

Again the agreement between the results obtained from the simulator and those in the literature is good, there are however a few anomalies. The results for $\rho^* = 0.85, T^* = 0.72$ and $\rho^* = 0.75, T^* = 0.81$ don't match very well, but this is due to these points lying in two-phase region which MD simulators don't work overly well. The other anomaly is the pressure calculated at $\rho^* = 0.85, T^* = 4.60$, the value from Chapela *et al.* does not match the trend and was probably supposed to be $\langle P^* \rangle = 17.43$. The validity of this data point and confirmation the two-phase behaviour of the first two anomalies was checked using another event-driven simulator, DynamO [4]. Good agreement was found between DynamO and this dissertation's event-driven simulator so these anomalies can be disregarded.

Now that the simulators are confirmed to be functioning correctly, comparisons can be made between continuous and discrete potentials. This dissertation will use the Lennard-Jones potential and attempt to find a suitable method to create an equivalent discrete potential. First, a comparison will be made with stepping methods already developed in the literature.

6.2 Previous Stepping Methods

There have been a number of methods used to convert continuous to discrete potentials previous to this dissertation. These discrete potentials are usually either handmade [1, 5, 6] or simply have the steps placed at even intervals [7]. Since Chapela *et al.* used ten steps

all discrete potentials created in this section will also use ten steps to allow comparisons to be made. A set of evenly spaced steps were created starting from a Barker-Henderson hard core diameter [8] (see Sec. 5.2.3) to a cutoff radius of 3σ. The cutoff radius value of 3σ was chosen as it is the truncation radius used in the force-driven simulation and all potentials generated in this chapter will use this cutoff. The heights of this evenly spaced potential was set so the areas under the discrete potential were the same as that for the continuous potential.

Figure 6.1 shows a comparison of results from a continuous potential to the evenly spaced step potential and the hand-made potential created by Chapela *et al.* It can be seen that evenly spaced steps do not reproduce the continuous potential results.

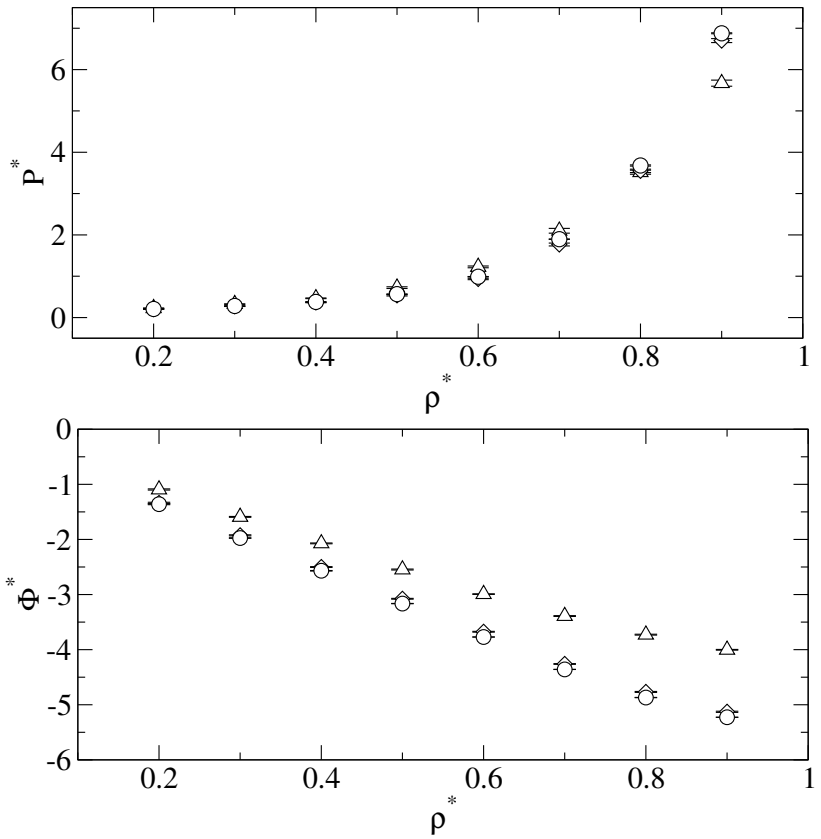

Figure 6.1: Plot of the reduced pressure (top) and potential energy (bottom) obtained from a continuous potential (circle); evenly-spaced steps (triangle); and the handmade steps from Chapela *et al.* (diamond).

The potential from Chapela *et al.* is significantly better and shows that it is indeed possible to create a stepped potential that can give similar results to a continuous potential. The results plotted here are the results measured using the techniques described in Secs. 4.2 and 4.4. Chapela *et al.* recommended using results measured from a converted RDF (Secs. 4.5 and 4.6); however, by doing this they sacrifice accuracy in pressure for accuracy in potential energy. As measuring values in the simulation and not from the RDF is more useful, these are the results that will be used from now on.

Creating a handmade potential is very time consuming, therefore there is a need to create an automatic stepping method. A number of techniques to create such a method will now be tested to investigate their effectiveness.

6.3 Stepping in Probability Versus Expected Force

The first method to create a stepped version of the Lennard-Jones potential was to step in equal probabilities (described in Sec. 5.2.1), starting with a core step calculated using the Barker-Henderson equivalent hard sphere diameter . The step heights were assigned using the equal probability method described in Sec. 5.3.1. The steps produced by this method is shown in Fig. 6.2. It can be seen that these steps do not follow the Lennard-Jones potential very well. The hard core and base of the well have been under-stepped. This is problematic as the core is fundamental to the freezing behaviour [9], and makes a large contribution to the pressure.

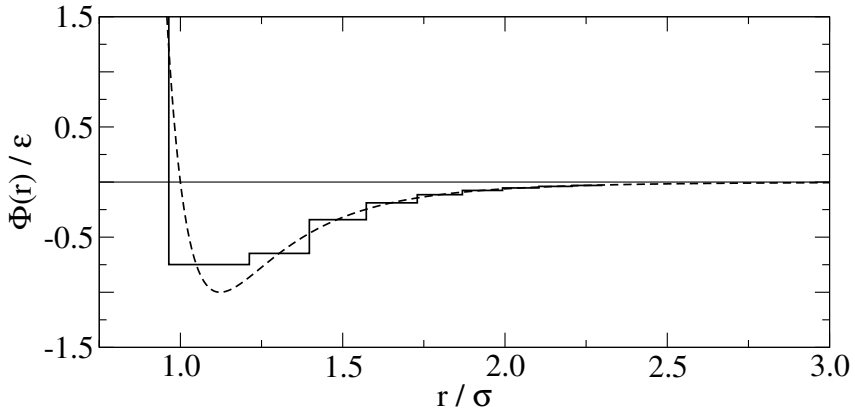

Figure 6.2: Plot of the steps produced by setting step positions in equal probabilities (solid) compared with the continuous Lennard-Jones potential (dashed).

Clearly a better method is needed. The reason the equal probability stepping failed is because even though the core is important there are very few particles there, hence it is under-represented. What is needed to improve this is to multiply the probability by a factor that is high at the core. The definition of the core is that the force is nearly infinite so this was used. This new method, stepping in equal contributions to the absolute value of the expected force is outlined in Sec. 5.2.2. The steps produced using this method is shown in Fig. 6.3. Again the innermost step was assigned using the Barker-Henderson hard sphere diameter, and the step heights were assigned to ensure equal probability. It can be seen that these steps match the Lennard-Jones potential significantly better than the probability stepping method.

The results of a simulation run with these steps is shown in Fig. 6.4. As can be seen these steps do not match the continuous potential results, this is probably due to the hard

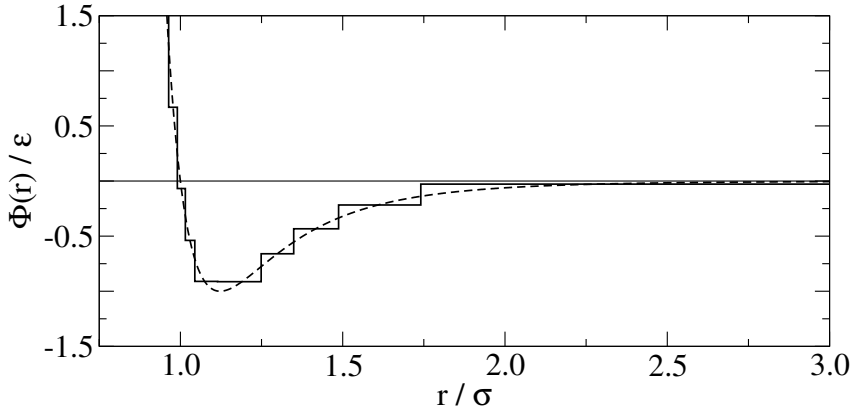

Figure 6.3: Plot of the steps produced by setting the step positions in equal magnitudes of the expected force (solid) compared with the continuous Lennard-Jones potential (dashed).

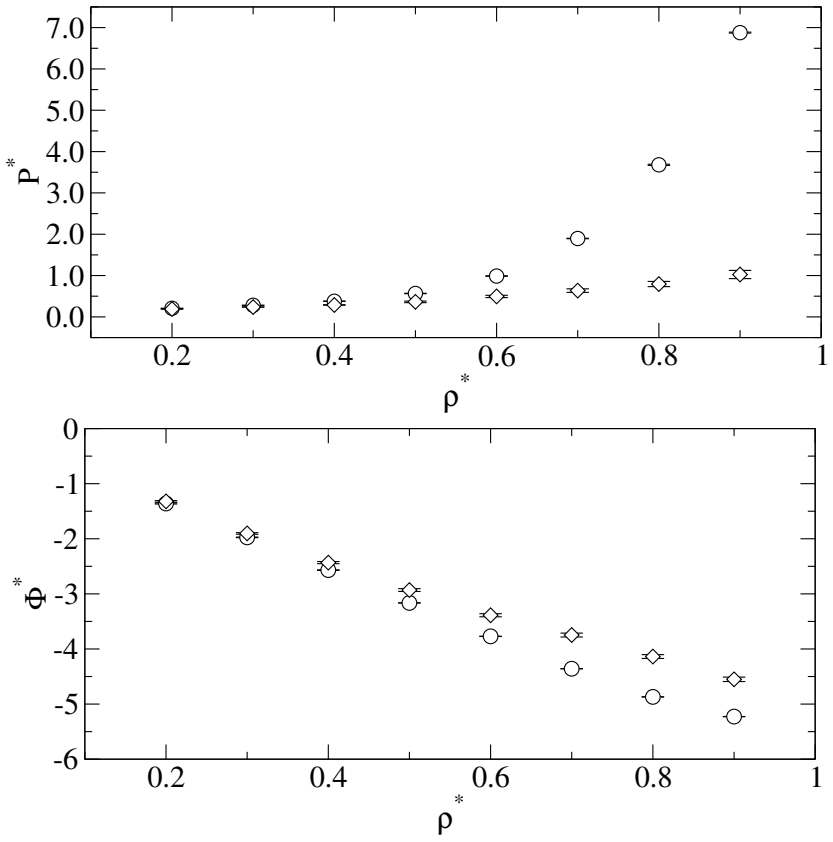

Figure 6.4: Plot of the reduced pressure (top) and potential energy (bottom) obtained from a continuous potential (circle) and steps set using the magnitude of the expected force (diamond).

core not being repulsive enough to keep the particles out of the core. This can be seen on the discontinuous RDF (see Fig. 6.5); there should be no particles inside the innermost step at $r \approx 0.96\sigma$, but the plot of the RDF clearly is non-zero well inside the core.

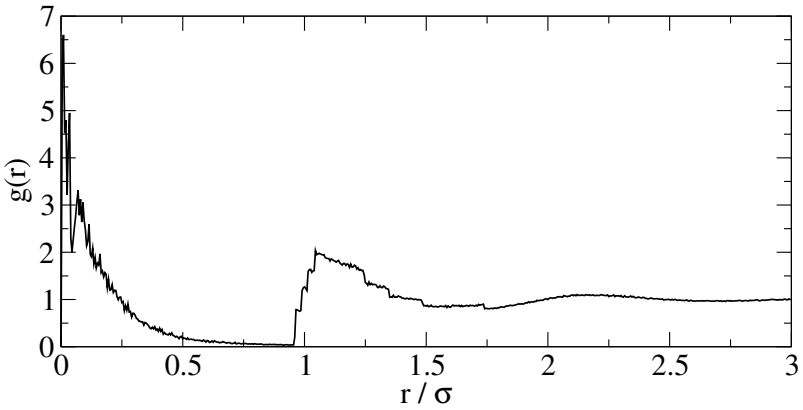

Figure 6.5: Plot of the RDF of the magnitude of expected force stepping without a hard core.

Therefore this method does not create a sufficiently "hard" core to keep particles outside each other. In the next, the placement of this hard core will be investigated

6.4 Hard Core Position

In the previous section, it was discovered that the core was sufficiently hard to ensure no particles could enter it. This was rectified by increasing the energy of the inner core to a very large value.

Until now the position of the inner core was selected using the Barker-Henderson equivalent hard sphere diameter; however, this may not be the best choice. The Barker-Henderson hard sphere diameter is only an approximation and was chosen in this dissertation due to its simplicity. An alternative method for selecting the hard core diameter is described in Sec. 5.2.3, and it places the core at a point where very few particles reach. Cores are placed at positions where four or five standard deviations (SD) of particles are located outside of the core. The results of this comparison is shown in Fig. 6.6.

It can be seen that $4\,\mathrm{SD}$ gives the best results for both pressure and potential energy, and hence, is the hard core position recommended by this dissertation.

6.5 Investigating Step Height Methods

A brief comparison was carried out to investigate the best method to set the heights of the steps. In Sec. 5.3, two methods were suggested to set the heights of the steps: either ensuring equal probability or equal potential energy. A set of steps for each were

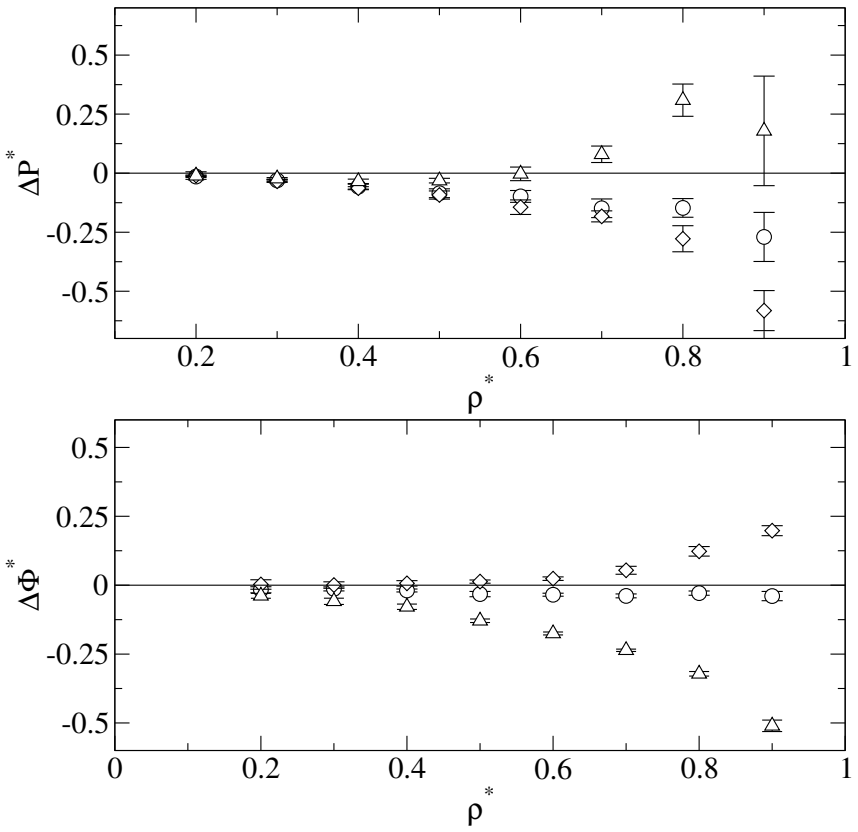

Figure 6.6: Plot of the error in reduced pressure(top) and potential(bottom) energy from the force-driven simulation obtained from a hard core placed using Barker-Henderson(triangle); 4 SD (circle); and 5 SD (diamond).

generated for $T^* = 1.5$ with a Barker-Henderson hard sphere diameter and the heights are shown in Table 6.4

There is very little difference in the heights of most of the steps therefore it is unlikely there is any significant difference between them. This was proven by running a simulation of both systems and the results were very similar.

6.6 Comparison with Previous Results

Now a complete stepping method has been created, it will be compared to those obtained by Chapela *et al.* Figure 6.7 shows the relative errors from the continuous potential for both stepping methods.

The potential created by Chapela *et al.* is slightly better that the one created in this dissertation for the pressure of the system, with this expected force stepping deviating from the force-driven simulators results at lower densities. The potential on the other hand is far better represented by the expected force stepping. The error from the continuous results is fairly constant with density and much lower than that for Chapela *et al.*

It should be noted here that the errors in both these stepping methods are very small

Table 6.4: Comparison of step energies produced by setting heights using probability and energy.

n	r_n	Φ_n	
		Probability	Energy
1	0.964	4.761	2.086
2	0.991	0.658	0.633
3	1.016	-0.074	-0.082
4	1.045	-0.542	-0.546
5	1.120	-0.918	-0.920
6	1.250	-0.910	-0.911
7	1.350	-0.659	-0.660
8	1.488	-0.433	-0.434
9	1.741	-0.217	-0.218
10	3.000	-0.028	-0.028

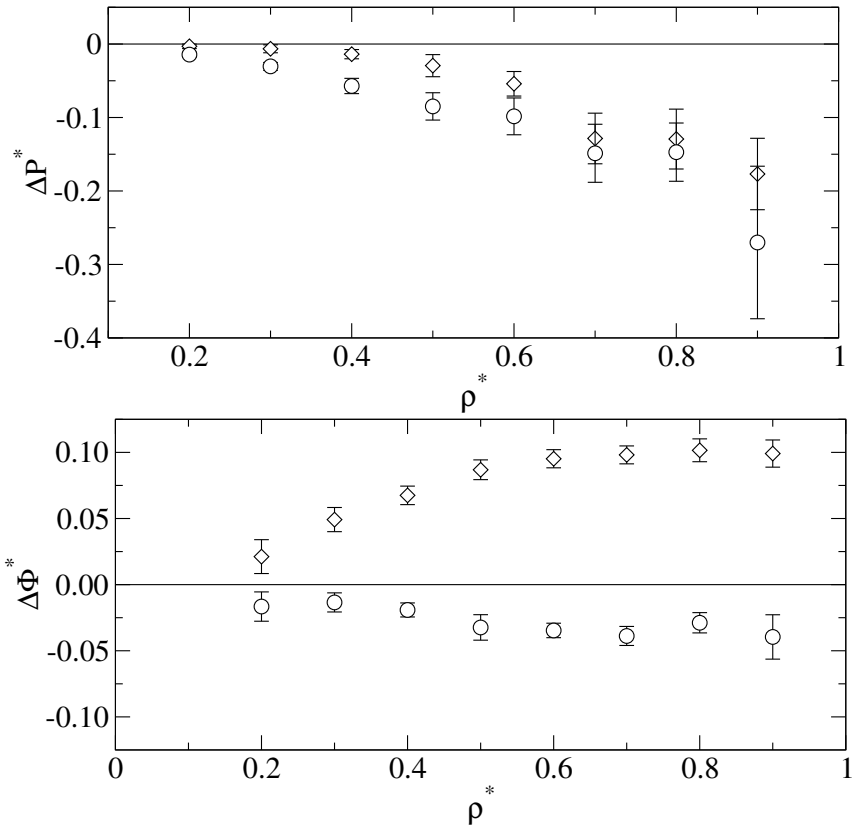

Figure 6.7: Plot of the error in the reduced pressure (top) and potential energy (bottom) from the continuous potential results for magnitude of the expected force steps (circle); and the steps from Chapela *et al.* (diamond).

when compared to the magnitudes of the values (Fig. 6.1 shows the similarity between Chapela *et al.* and the continuous potential results).

6.7 Temperature Comparisons

The advantage of the current stepping system is that all the methods are dependant on the temperature of the system. This should mean that the results of the simulation deteriorate slower than those taken from Chapela *et al.*.

The error in potential energy from the force-driven simulation at a number of temperatures is shown in Fig. 6.8.

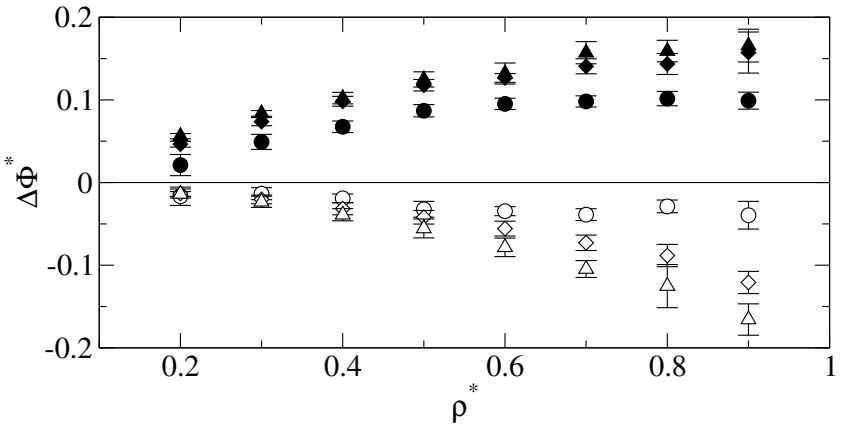

Figure 6.8: Temperature comparison of errors in potential energy obtained from Chapela *et al.* steps (filled), and this dissertation's steps (unfilled) at temperatures of $T^* = 1.5$ (circle), $T^* = 3.0$ (diamond) and $T^* = 4.5$ (triangle).

It can be seen that stepping method developed in this dissertation actually increases in error faster than potential created by Chapela *et al.*. As temperature increases the steps are more densely concentrated at the inner core which is correct; this implies that it is the height determining aspect of the stepping method that is to blame for this deterioration.

The plot for pressure is shown in Fig. 6.9. Unlike the potential energy there is no discernible trend in the data for increasing temperature. This should be the case as the steps were set to ensure probability was the same in both discrete and continuous potentials. It was shown in Sec. 5.3.1 that this was equivalent to setting the second virial coefficient the same, so the pressure should be maintained more accurately than the energy.

If any trend can be identified it would be that the error at high density seems to be reducing with temperature. This is unusual as the higher order virial coefficients should become more important at high temperature [10]. However, the error bars significantly larger than those for potential energy so there is the possibility this trend is simply statistical error.

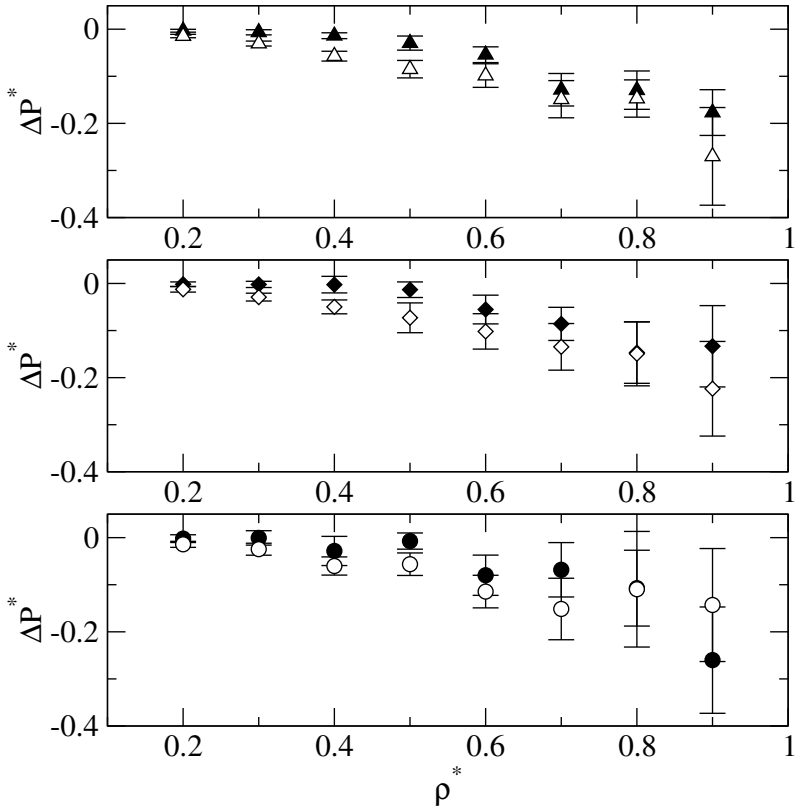

Figure 6.9: Temperature comparison of error in pressure obtained from Chapela *et al.* steps (filled), and this dissertation's steps (unfilled) at temperatures of $T^* = 1.5$ (triangle, top), $T^* = 3.0$ (diamond, middle) and $T^* = 4.5$ (circle, bottom).

6.8 Summary

Now that the techniques for setting the stepping parameters have been investigated, the best method is outlined here. The optimal method for setting the step positions is to ensure that the magnitude of the expected force is equal in each step interval. The heights of the steps should be set to ensure the probability and hence, the second virial coefficient, of the continuous and discrete potentials are the same. The inner hard core should be set at a location that four standard deviations of particles do not reach.

The steps created by this method are compared with those created by Chapela *et al.* in Fig. 6.10. The steps are similar, both concentrate their steps at the core, though those of Chapela *et al.* are further in than those created by this method. The results produced by both methods are very similar (see Fig. 6.7); however, the steps created using the above method have the advantage of that they are automatic.

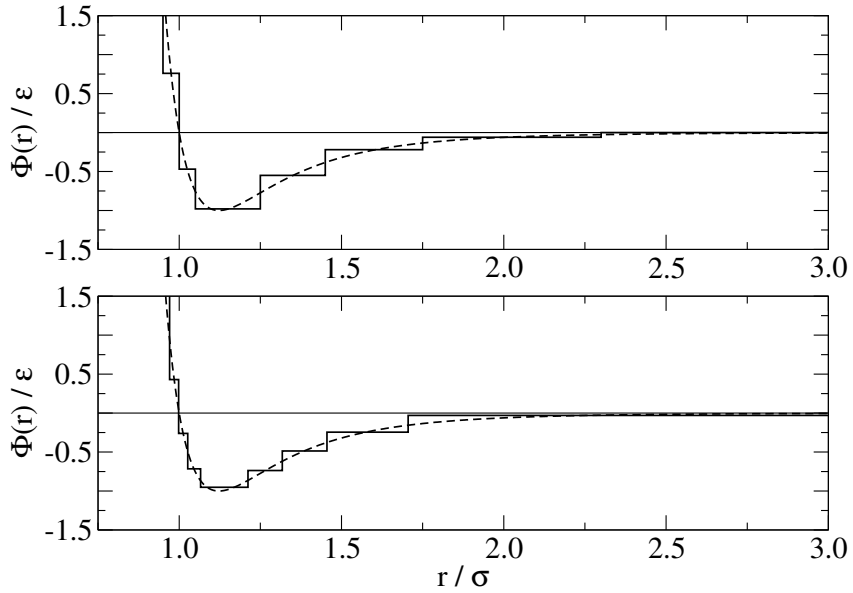

Figure 6.10: Comparison of the steps created by Chapela *et al.* (top) and those created in this dissertation (bottom) at a temperature of $T^* = 1.5$.

6.9 References

[1] Chapela, G.; Scriven, L. E.; Davis, H. T. Molecular Dynamics for Discontinuous Potential. IV. Lennard-Jonesium. *J. Chem. Phys.* **1989**, *91*, 4307, DOI: 10.1063/1.456811.

[2] Limbach, H.; Arnold, A.; Mann, B.; Holm, C. ESPResSo - An Extensible Simulation Package for Research on Soft Matter Systems. *Comput. Phys. Commun.* **2006**, *174*, 704 –727, DOI: 10.1016/j.cpc.2005.10.005.

[3] Lue, L. Collision Statistics, Thermodynamics, and Transport Coeffiecients of Hard Hyperspheres in Three, Four, and Five Dimensions. *J. Chem. Phys.* **2005**, *122*, 044513, DOI: 10.1063/1.1834498.

[4] Bannerman, M. N.; Sargant, R.; Lue, L. DynamO: A Free $\mathcal{O}$(N) General Event-Driven Molecular Dynamics Simulator. *J. Comput. Chem.* **2011**, *32*, 3329–3338, DOI: 10.1002/jcc.21915.

[5] Unlu, O.; Gray, N. H.; Gerek, Z. N.; Elliott, J. R. Transferable Step Potentials for the Straight-Chain Alkanes, Alkenes, Alkynes, Ethers, and Alcohols. *Ind. Eng. Chem. Res.* **2004**, *43*, 1788–1793, DOI: 10.1021/ie034036m.

[6] Elliot Jr., J. R. Optimized Step Potential Models for n-Alkanes and Benzene. *Fluid Phase Equilib.* **2002**, *194-197*, 161–168, DOI: 10.1016/S0378-3812(01)00664-1.

[7] Chapela, G.; Rio, F. del; Benavides, A. L.; Alejandre, J. Discrete Perturbation Theory Applied to Lennard-Jones and Yukawa Potentials. *J. Chem. Phys.* **2010**, *133*, 234107.

[8] Barker, J. A.; Henderson, D. Perturbation Theory and Equation of State for Fluids: II. A Successful Theory of Liquids. *J. Chem. Phys.* **1967**, *47*, 4714–4721.

[9] Alder, B. J.; Wainwright, T. E. Phase Transition for a Hard Sphere System. *J. Chem. Phys.* **1957**, *27*, 1208–1209, DOI: 10.1063/1.1743957.

[10] Sun, T.; Teja, A. S. An Equation of State for Real Fluids Based on the Lennard-Jones Potential. *J. Phys. Chem.* **1996**, *100*, 17365–17372, DOI: 10.1021/jp9620476.

CHAPTER

SEVEN

CONCLUSIONS AND FUTURE WORK

7.1 Conclusions

The aims of this dissertation were to create a working force-driven and event-driven simulator, and to create a general method for converting continuous to discrete potentials. Both of these aims were achieved in this dissertation.

A large part of this dissertation was the creation of the simulators required to test the effectiveness of any conversion method. Both the simulators work correctly and include many of the optimisation techniques (with the exception of a neighbour list in the event-driven simulation) available to either simulation method. This ensured that a reasonable size system (864 particles, 1.5 million collisions) could be simulated in a relatively short period of time (< 30 mins) on an average desktop computer. Due to this a large number of comparisons, each repeated a number of times, could be undertaken during the timescale of this project.

A general method was created in this dissertation to convert a continuous to discrete potential. The method is outlined as follows. The step positions were set to have equal magnitudes of the expected force (see Sec. 5.2.2). Meanwhile the step energies were placed to ensure equal probabilities as the continuous potential (Sec. 5.3.1). The position of the hard core is set at a position where four standard deviations of particles are outside of that location.

This method successfully emulates the behaviour of the continuous Lennard-Jones potential over a range of temperatures ($T^* = 1.5 - 4.5$) and densities ($\rho^* = 0.2 - 0.9$). It also gives comparable results to the hand-made steps of Chapela *et al.* [1] and has the major advantage that it can be implemented into the simulator itself. The event-driven simulator used in this dissertation generated the steps using the outlined method at the start of every simulation run. This means that parameters such as the number of steps can be changed easily and with no additional work.

With the automatic stepping procedure developed in this work, it is possible to convert

the large number of advanced continuous potentials in the literature to discrete potentials. This could allow accurate predictions of thermodynamic properties for a wide range of fluids and develop a deeper understanding of molecular interactions.

7.2 Suggestions for Future Work

While the stepping method presented in this dissertation is a significant improvement over any existing method it would still benefit from further work.

The most important problem of this method is that the core needs to be manually hardened and its placement needs to be done separately. Ideally, these should be taken into account by the methods for setting set positions and heights. Therefore although this method produces very similar results to continuous potentials, there is still room for improvement in both the step positioning and determining the heights of the steps.

If a radial distribution function generated from a force-driven simulation could be implemented into the method, the validity of the positioning and height determining methods could be verified. Both of these methods implicitly assume that the RDF is one, so the inclusion of the RDF should give improved results.

While ten steps were used to model the continuous potential in this study, this was done purely so a comparison could be made to Chapela *et al.*. An investigation could also be carried out to find the optimal number of steps; clearly more steps would model the continuous potential better, but the increase in computational cost required for this increase could be studied.

The aim of this general stepping method is that it is supposed to applicable to any potential. In this dissertation it was only compared to Lennard-Jones potential during the method's development; however it should compared against a wide range of alternative continuous potentials (such as CHARMM [2]) to check whether it succeeds at this aim.

7.3 References

[1] Chapela, G.; Scriven, L. E.; Davis, H. T. Molecular Dynamics for Discontinuous Potential. IV. Lennard-Jonesium. *J. Chem. Phys.* **1989**, *91*, 4307, DOI: 10.1063/1.456811.

[2] MacKerell, A. D. et al. All-Atom Empirical Potential for Molecular Modeling and Dynamics Studies of Proteins. *J. Phys. Chem. B* **1998**, *102*, 3586–3616, DOI: 10.1021/jp973084f.

APPENDIX

A

DERIVATION OF COLLISION DYNAMICS FOR STEPPED POTENTIALS

Considering a collision between particles i and j, each with mass, m with a step energy difference of $\Delta\Phi$, the conservation of momentum is shown in Eq. (A.0.1). Here the prime indicates post-collision values.

$$m\mathbf{v}_i + m\mathbf{v}_j = m\mathbf{v}_i' + m\mathbf{v}_j' \tag{A.0.1}$$

The momentum change of each particle must occur along the separation vector between the two particles, which can be expressed by:

$$m\mathbf{v}_i - m\mathbf{v}_i' = -(m\mathbf{v}_j - m\mathbf{v}_j') = -A\hat{\mathbf{r}}_{ij} \tag{A.0.2}$$

where A is an arbitrary coefficient.

Energy must also be conserved in the system so Eq. (A.0.3) must also apply. This can be rewritten to Eqs. (A.0.4) and (A.0.5)

$$\frac{1}{2}mv_i^2 + \frac{1}{2}mv_j^2 = \frac{1}{2}mv_i'^2 + \frac{1}{2}mv_j'^2 + \Delta\Phi \tag{A.0.3}$$

$$v_i^2 - v_i'^2 + v_j^2 - v_j'^2 - \frac{2}{m}\Delta\Phi = 0 \tag{A.0.4}$$

$$(\mathbf{v}_i - \mathbf{v}_i') \cdot (\mathbf{v}_i + \mathbf{v}_i') + (\mathbf{v}_j - \mathbf{v}_j') \cdot (\mathbf{v}_j + \mathbf{v}_j') - \frac{2}{m}\Delta\Phi = 0 \tag{A.0.5}$$

Equation (A.0.2) can now be substituted into Eq. (A.0.5) to give Eq. (A.0.6).

$$\frac{A}{m}\hat{\mathbf{r}}_{ij}(\mathbf{v}_j - \mathbf{v}_i + \mathbf{v}_j' - \mathbf{v}_i') - \frac{2}{m}\Delta\Phi = 0 \tag{A.0.6}$$

Equation (A.0.2) and the definition of the separation velocity vector ($\mathbf{v}_{ij} = \mathbf{v}_i - \mathbf{v}_j$) can be substituted into Eq. (A.0.6) to give Eq. (A.0.7).

$$-\frac{A^2}{m} - A\hat{\mathbf{r}}_{ij} \cdot \mathbf{v}_{ij} - \Delta\Phi = 0 \tag{A.0.7}$$

This is a quadratic equation in terms of A therefore it's roots must be given by equation:

$$A = -\frac{m}{2}\left((\mathbf{v}_{ij} \cdot \hat{\mathbf{r}}_{ij}) \pm \sqrt{(\mathbf{v}_{ij} \cdot \hat{\mathbf{r}}_{ij})^2 - \frac{4}{m}\Delta\Phi}\right) \tag{A.0.8}$$

From Eq. (A.0.2), the change in velocity of each particle is given in Eqs. (A.0.9)

$$\Delta\mathbf{v}_i = \frac{A}{m}\hat{\mathbf{r}}_{ij} \tag{A.0.9a}$$

$$\Delta\mathbf{v}_j = -\frac{A}{m}\hat{\mathbf{r}}_{ij} \tag{A.0.9b}$$